

Aircraft navigation based on differentiation-integration observer

Xinhua Wang¹, Lilong Cai²

¹Department of Electrical and Electronic Engineering, University of Nottingham,
University Park, Nottingham, NG7 2RD, United Kingdom (Email: xinhua.wang1@nottingham.ac.uk)

²Department of Mechanical and Aerospace Engineering,
Hong Kong University of Science and Technology, Hong Kong, China (Email: melcai@ust.hk)

Abstract: In this paper, a generalized differentiation-integration observer is presented based on sensors selection. The proposed differentiation-integration observer can estimate the multiple integrals and high-order derivatives of a signal, synchronously. The parameters selection rules are presented for the differentiation-integration observer. The theoretical results are confirmed by the frequency-domain analysis. The effectiveness of the proposed observer are verified through the numerical simulations on a quadrotor aircraft: i) through the differentiation-integration observer, the attitude angle and the uncertainties in attitude dynamics are estimated synchronously from the measurements of angular velocity; ii) a control law is designed based on the observers to drive the aircraft to track a reference trajectory.

Keywords: Differentiation-integration observer, multiple integrals, derivatives, quadrotor aircraft

1 Introduction

Integration and differentiation are important components in almost all industrial applications. Their problems are of estimating the values $I(a) = \int_0^t \cdots \int_0^s a(\sigma) d\sigma \cdots d\tau$ and $D_i(a) = \frac{d^i a(t)}{dt^i}$. The positions, velocities and accelerations are the important elements for many systems. In an inertial navigation system (INS), the inertial measurement unit (IMU) typically measures the three-axial angular velocity and the three-axial linear acceleration, respectively. To obtain the attitude angle and angular acceleration of the device, the angular velocity signals are integrated and differentiated, respectively. For a long-time navigation, the drift phenomenon of INS is mainly brought out by the usual integration methods. They cannot restrain the effect of stochastic noise (especially non-zero mean noise). The noise leads to the accumulation of additional drift in the integrated signal.

The algorithms of differentiation and integration have been studied by a number of researchers [1]-[23]. The linear high-gain differentiators [2, 3] can provide the estimations of signal derivatives. In another study, a differentiator via high-order sliding modes algorithm was proposed [4, 5]. In [6]-[9], the continuous nonlinear differentiators based on finite-time stability were presented to provide the smooth estimations of signal derivatives. However, the differentiators did not consider the signal integral estimations [1]-[10].

Some numerical methods were proposed to estimate signal integral [11]: i) The trapezoidal rule; ii) Simpson's rule. For the above numerical integrating methods, if stochastic non-zero mean noise exists in signal, then such noise leads to the accumulation of additional drift in the integrated signal. As we known, the desired integral operators $1/s$ and $1/s^2$ are irrational, and they cannot be calculated directly. Some approximated methods were presented to estimate signal integral: IIR digital integrator [12, 13], the Newton-Cotes digital integrators [14], precision digital integrator [15], non-inverting integrator [16], the developed infinite impulse response digital integrators [17,

18], the low-frequency differential differentiators [19, 20]. However, for the aforementioned integrators [12]-[20], only onefold integral was calculated, and the synchronous estimations of derivatives and integrals were not considered. Some integrators were implemented using the hardware units, where the circumstances usually affect the parameters, for instance, the temperature in the circuit changes. Thus, the estimation precisions are affected adversely. Moreover, they are easily infected by stochastic noise, and the drift phenomena are inevitable in such systems. In order to reduce the noise, additional filters must be added. In [21] and [22], a fractional-order integrator has been presented, and a rational transfer function was proposed to approximate the irrational integrator $1/s^m$. However, the limitation of $0 < m < 1$ limits its application. The onefold and double integrals are necessary in many navigation systems. The Kalman filter can estimate position and velocity from the acceleration measurement [23]. However, it is supposed that the process noise covariance and measurement noise covariance are required to be zero-mean Gaussian distributed, and the process noise covariance is uncorrelated to the estimation error. These assumptions are different from the practical noise in signal. The inaccurate noise requirements may lead to the estimate drifts of position and velocity.

In [24], a nonlinear double-integral observer was presented to estimate synchronously the onefold and double integrals of a signal, and a generalized multiple integrator was designed to estimate the multiple integrals [25]. In [26], a nonlinear integral-derivative observer was proposed to estimate synchronously the integral and derivative of a signal. The parameters selection is required to be satisfied with Routh-Hurwitz Stability Criterion and the iterative equation relations. Moreover, the nonlinear observers in [26] are complicated and difficult to compute. The existing hardware computational circumstances affect the nonlinear function implementations adversely, i.e., the implementation of the these nonlinear observers in many digital processors is difficult. Due to the existence of such many parameters, the parameters regulation of this nonlinear observer is complicated.

In this paper, a generalized high-order linear differentiation-integration observer is presented, which can estimate the multiple integrals and high-order derivatives of a signal, synchronously. Different from the nonlinear observer theories in [26], the classical theory of linear system can be used to prove its stability, and the Bode plots are adopted to analyze its robustness. The parameters selection become relaxed, and it is only required to be satisfied with a simple Hurwitz condition. The existing layout of perturbation parameters in singular perturbation technique [27, 28] is only suitable to estimate the derivatives of a signal. In this differentiation-integration observer, a new distribution of perturbation parameters is presented for the requirement of synchronous estimation of the integrals and derivatives. The parameters selection rules and robustness analysis for the differentiation-integration observer are presented based on frequency-domain analysis.

Finally, we use the mathematical model and reference trajectory of the quadrotor aircraft described in [29], and the computational analysis and simulation are presented to observe the performances of the proposed observer. Usually controlling a quadrotor aircraft to track a reference trajectory needs the information of the position and attitude. Quadrotor aircraft control has been an active area of investigation for several years [30]-[34]. However, these strategies are dependent on the accurate model, and all the states are required to be known. In [29], although the uncertainties were considered, the attitude angle was supposed to be known. For the system of a quadrotor aircraft, we consider that the information of flying velocity and attitude angle is not

provided. Moreover, quadrotor aircrafts are underactuated mechanical systems, and aerodynamic disturbance, unmodelled dynamics and parametric uncertainties are not avoidable in modeling. Based on the presented differentiation-integration observer, this paper provides a tracking control method for a quadrotor aircraft by using the measurements of position and angular velocity. The unknown velocity, attitude angle and uncertainties are reconstructed by the observers. Furthermore, a controller is designed to stabilize the flight dynamics.

2 Generalized differentiation-integration observer

2.1 Configuration of differentiation-integration observer

The goal of the differentiation-integration observer design is to estimate the needed states from the different sensors, for instance:

1) *Estimation of velocity and acceleration from position:* In a GPS, position $p(t)$ is known, we want to obtain the velocity and acceleration. Therefore, we expect to design an observer to estimate the first-order derivative $\dot{p}(t)$ and second-order derivative $\ddot{p}(t)$ of the signal $p(t)$, synchronously. The observer should include the state $x = (x_1, x_2, x_3)$, and the configuration of the observer is described as follow:

$$\begin{aligned}\dot{x}_1 &= x_2; \dot{x}_2 = x_3; \\ \dot{x}_3 &= f(x_1 - p(t), x_2, x_3)\end{aligned}\tag{1}$$

where the first state x_1 of observer (1) points to the input signal $p(t)$. If the state x_1 estimates $p(t)$, and the system is stable, then, from the integral-chain relations of x_1, x_2, x_3 in system (1), the first-order and second-order derivatives of signal $p(t)$ can be estimated, synchronously.

2) *Estimation of attitude angle and angular acceleration from angular velocity:* In an IMU, angular velocity $\omega(t)$ can be measured directly. We want to obtain the attitude angle and angular acceleration. Therefore, we expect to design an observer to estimate the integral $\int_0^t \omega(\sigma) d\sigma$ and the derivative $\dot{\omega}(t)$ of signal $\omega(t)$, synchronously. The observer should include the state $x = (x_1, x_2, x_3)$, and the configuration of the observer is shown as follow:

$$\begin{aligned}\dot{x}_1 &= x_2; \dot{x}_2 = x_3; \\ \dot{x}_3 &= f(x_1, x_2 - a(t), x_3)\end{aligned}\tag{2}$$

where the second state x_2 of observer (2) points to the input signal $\omega(t)$. If the state x_2 estimates $\omega(t)$, and the system is stable, then, from the integral-chain relations of x_1, x_2, x_3 in system (2), the onefold integral and first-order derivative of signal $\omega(t)$ can be estimated, synchronously.

3) *Estimation of position and velocity from acceleration:* In the third case, the acceleration $a_c(t)$ is measured by a accelerometer, and we want to obtain the position and the velocity. Therefore, we expect to design an observer to estimate the onefold integral $\int_0^t a_c(\sigma) d\sigma$ and the double integral $\int_0^t \int_0^s a_c(\sigma) d\sigma d\tau$ of signal $a_c(t)$, synchronously. The observer should include the state $x = (x_1, x_2, x_3)$, and the configuration of the observer is described as follow:

$$\begin{aligned}\dot{x}_1 &= x_2; \dot{x}_2 = x_3; \\ \dot{x}_3 &= f(x_1, x_2, x_3 - a(t))\end{aligned}\quad (3)$$

where the third state x_3 of observer (3) points to signal $a_c(t)$. If the state x_3 estimates $a_c(t)$, and the system is stable, then, from the integral-chain relations of x_1, x_2, x_3 in system (3), the onefold and double integrals of signal $a_c(t)$ can be estimated, synchronously.

4) *Generalized cases:* Generally, for signal $a(t)$ measured from a sensor, we expect to design an observer to estimate the multiple integrals up to $(p - 1)$ th multiple and high-order derivatives up to $(n - p)$ th order, synchronously, where $p \in \{1, \dots, n\}$ corresponds to different sensors. Let the i th-multiple integral of signal $a(t)$ be $I_{p-i}(t) = \underbrace{\int_0^t \dots \int_0^s}_{i} a(\sigma) \underbrace{d\sigma \dots d\tau}_i$, where $i \in \{1, \dots, p - 1\}$;

$I_p(t) = a(t)$; and the $(r - p)$ th-order derivative of signal $a(t)$ be $I_r(t) = a^{(r-p)}(t)$, $r = p + 1, \dots, n$. The observer should include the state $x = (x_1, \dots, x_p, \dots, x_n)$, and the configuration of the observer is presented as follow:

$$\begin{aligned}\dot{x}_1 &= x_2 \\ &\dots \\ \dot{x}_p &= x_{p+1} \\ &\dots \\ \dot{x}_n &= f(x_1, \dots, x_p - a(t), \dots, x_n)\end{aligned}\quad (4)$$

where the p -th state x_p of observer (4) points to signal $a(t)$. If the state x_p estimates $a(t)$, and the system is stable, then, from the integral-chain relations of $x_1, \dots, x_p, \dots, x_n$ in system (4), the multiple integrals and high-order derivatives of signal $a(t)$ can be estimated, synchronously.

The goals of the observation are: 1) synchronous estimation of multiple integrals and high-order derivatives of a signal; 2) regulation of low-pass frequency bandwidth through the ease of parameter selection, and sufficient high-frequency noise rejection.

2.2 Existence conditions of Hurwitz characteristic polynomial

Before constructing the explicit form of the differentiation-integration observer (4), we propose a n th-order characteristic polynomial

$$s^n + k_n s^{n-1} + \dots + \frac{k_p}{\varepsilon^{p-c(p)}} s^{p-1} + \dots + k_2 s + k_1 \quad (5)$$

where, $p \in \{1, \dots, n\}$, and

$$c(p) = \begin{cases} 1, & p = 1 \\ 0, & p > 1 \end{cases} \quad (6)$$

Here, the Hurwitz conditions of the polynomial (5) is considered. The polynomial is used for construct a linear differentiation-integration observer. We consider the following question: For the

arbitrary $\varepsilon \in (0, 1)$, by selecting parameters k_1, \dots, k_n , whether can all the positive integers n and $p \in \{1, \dots, n\}$ make the polynomial (5) Hurwitz?

For instance, we can find that: 1) for the arbitrary $\varepsilon \in (0, 1)$, when we select $n = 4$ and $p = 2$, the polynomial (5) cannot be Hurwitz; 2) for the arbitrary $\varepsilon \in (0, 1)$, when $n = 5$ and $p \in \{2, 3, 4, 5\}$, the polynomial (5) cannot be Hurwitz.

For the arbitrary $\varepsilon \in (0, 1)$, the following lemma presents the selections of n and p to make polynomial (5) Hurwitz.

Lemma 1: For the arbitrary $\varepsilon \in (0, 1)$, in the following cases, the polynomial (5) can be Hurwitz:

a) $n \in \{1, 2, \dots\}$ and $p = 1$: $k_i > 0$ (where $i = 1, \dots, n$) are selected such that the polynomial $s^n + \sum_{i=1}^n k_i s^{i-1}$ is Hurwitz.

b) $n = 2$ and $p = 2$: $k_1 > 0, k_2 > 0$.

c) $n = 3$ and $p \in \{2, 3\}$: when $p = 2$, $k_1 > 0, k_3 > 0$ and $k_2 > \varepsilon^2 \frac{k_1}{k_3}$; when $p = 3$, $k_1 > 0, k_3 > 0$ and $k_2 > \varepsilon^3 \frac{k_1}{k_3}$.

d) $n = 4$ and $p = 3$: $k_1 > 0, k_4 > 0, k_3 > \varepsilon^3 \frac{k_2}{k_4}$ and $k_2 > \varepsilon^3 \frac{k_4^2 k_1 + k_2^2}{k_4 k_3}$.

The proof of Lemma 1 is presented in Appendix.

2.3 Design of generalized differentiation-integration observer

In the following, the singular perturbation technique will be used to design a generalized differentiation-integration observer, and Theorem 1 is presented as follow.

Theorem 1: For system

$$\begin{aligned} \dot{x}_i &= x_{i+1}; i = 1, \dots, n-1 \\ \varepsilon^{n+1-c(p)} \dot{x}_n &= - \sum_{i=1, i \neq p}^n k_i \varepsilon^{i-c(p)} x_i - k_p (x_p - a(t)) \end{aligned} \quad (7)$$

where, $p \in \{1, \dots, n\}$, and

$$c(p) = \begin{cases} 1, & p = 1 \\ 0, & p > 1 \end{cases} \quad (8)$$

$a(t)$ is the signal that can be directly measured, and it is continuous, integrable and $(n-p+1)$ th-order derivable. Let $a_{p-i}(t) = \underbrace{\int_0^t \dots \int_0^s}_{i} a(\sigma) \underbrace{d\sigma \dots d\tau}_i$, $i \in \{1, \dots, p-1\}$; $a_p(t) = a(t)$; $a_r(t) =$

$a^{(r-p)}(t)$, $r = p+1, \dots, n$; $\varepsilon \in (0, 1)$ is the perturbation parameter; $k_1, \dots, \frac{k_p}{\varepsilon^{p-c(p)}}, \dots, k_n > 0$ are selected such that $s^n + k_n s^{n-1} + \dots + \frac{k_p}{\varepsilon^{p-c(p)}} s^{p-1} + \dots + k_2 s + k_1$ is Hurwitz, then the following conclusions hold:

$$\lim_{\varepsilon \rightarrow 0} x_i = a_i(t), \text{ for } i \in \{1, \dots, n\} \quad (9)$$

and observer (7) is stable.

Proof: The Laplace transformation of (7) can be calculated as follow:

$$\begin{aligned} sX_i(s) &= X_{i+1}(s); i = 1, \dots, n-1 \\ \varepsilon^{n+1-c(p)} sX_n(s) &= - \sum_{i=1, i \neq p}^n k_i \varepsilon^{i-c(p)} X_i(s) - k_p (X_p(s) - A(s)) \end{aligned} \quad (10)$$

where $X_i(s)$ and $A(s)$ denote the Laplace transformations of x_i and $a(t)$, respectively, and s denotes Laplace operator. From (10), we obtain

$$X_i(s) = \frac{X_j(s)}{s^{j-i}}, i = 1, \dots, n, j \in \{1, \dots, n\} \quad (11)$$

Therefore, Eq. (10) can be written as

$$s^{n-j+1} \varepsilon^{n+1-c(p)} X_j(s) = - \sum_{i=1, i \neq p}^n k_i \varepsilon^{i-c(p)} \frac{X_j(s)}{s^{j-i}} - k_p \left(\frac{X_j(s)}{s^{j-p}} - A(s) \right) \quad (12)$$

Then, it follows that

$$\frac{X_j(s)}{A(s)} = \frac{k_p}{s^{n-j+1} \varepsilon^{n+1-c(p)} + \sum_{i=1, i \neq p}^n \frac{k_i \varepsilon^{i-c(p)}}{s^{j-i}} + \frac{k_p}{s^{j-p}}} \quad (13)$$

i.e.,

$$\frac{X_j(s)}{A(s)} = \frac{s^{j-1} k_p}{s^n \varepsilon^{n+1-c(p)} + \sum_{i=1, i \neq p}^n s^{i-1} k_i \varepsilon^{i-c(p)} + s^{p-1} k_p} \quad (14)$$

Therefore, we obtain

$$\lim_{\varepsilon \rightarrow 0} \frac{X_j(s)}{A(s)} = s^{j-p} \quad (15)$$

where $j \in \{1, \dots, n\}$ and $p \in \{1, \dots, n\}$. It means that the state x_i approximates $a_i(t)$, for $1 \leq i \leq n$.

From Eq. (14), the characteristic polynomial of observer (7) is

$$s^n + \sum_{i=1, i \neq p}^n \frac{k_i}{\varepsilon^{n-i+1}} s^{i-1} + \frac{k_p / \varepsilon^{p-c(p)}}{\varepsilon^{n-p+1}} s^{p-1} \quad (16)$$

Importantly, in order to make the system stable, the characteristic polynomial is required to be Hurwitz. It is equivalent that

$$s^n + \sum_{i=1, i \neq p}^n k_i s^{i-1} + \frac{k_p}{\varepsilon^{p-c(p)}} s^{p-1} \quad (17)$$

should be Hurwitz. This concludes the proof. ■

From Theorem 1, we find that: the state x_p estimates the signal $a(t)$, x_i estimates the $(p-i)$ th-multiple integral of signal $a(t)$, where $i \in \{1, \dots, p-1\}$; x_r estimates the $(r-p)$ th-order derivative of signal $a(t)$, where $r = p+1, \dots, n$.

2.4 Explicit forms of differentiation-integration observers

From Theorem 1 and Lemma 1, the explicit forms of generalized differentiation-integration observer can be deduced, and a corollary is presented as follow. It includes: high-order differentiator, onefold integrator, differentiation-integration observer, double integrator, differentiation and double-integration observer.

Corollary 1: The following differentiation-integration observers exist:

i) High-order differentiator [35] (where $n \in \{1, 2, \dots\}$ and $p = 1$):

$$\begin{aligned} \dot{x}_i &= x_{i+1}; i = 1, \dots, n-1 \\ \varepsilon^n \dot{x}_n &= -k_1(x_1 - a(t)) - \sum_{i=2}^n k_i \varepsilon^{i-1} x_i \end{aligned} \quad (18)$$

where, $\varepsilon \in (0, 1)$; $k_i > 0$ ($i = 1, \dots, n$) are selected such that the polynomial $s^n + \sum_{i=1}^n k_i s^{i-1}$ is Hurwitz. For differentiator (18), the following conclusions hold:

$$\lim_{\varepsilon \rightarrow 0} x_i = a^{(i-1)}(t), \text{ for } i \in \{1, \dots, n\} \quad (19)$$

It can estimate the derivatives of signal $a(t)$ up to $(n-1)$ th order.

ii) Onefold integrator (where $n = 2$ and $p = 2$):

$$\begin{aligned} \dot{x}_1 &= x_2 \\ \varepsilon^3 \dot{x}_2 &= -k_1 \varepsilon x_1 - k_2(x_2 - a(t)) \end{aligned} \quad (20)$$

where, $\varepsilon \in (0, 1)$; $k_1 > 0, k_2 > 0$. The following conclusions hold:

$$\lim_{\varepsilon \rightarrow 0} x_1 = \int_0^t a(\tau) d\tau, \lim_{\varepsilon \rightarrow 0} x_2 = a(t) \quad (21)$$

It can estimate the onefold integral of signal $a(t)$.

iii) Differentiation-integration observer (where $n = 3$ and $p = 2$):

$$\begin{aligned} \dot{x}_1 &= x_2 \\ \dot{x}_2 &= x_3 \\ \varepsilon^4 \dot{x}_3 &= -k_1 \varepsilon x_1 - k_2(x_2 - a(t)) - k_3 \varepsilon^3 x_3 \end{aligned} \quad (22)$$

where, $\varepsilon \in (0, 1)$; $k_1 > 0, k_3 > 0$ and $k_2 > \varepsilon^2 \frac{k_1}{k_3}$. The following conclusions hold:

$$\lim_{\varepsilon \rightarrow 0} x_1 = \int_0^t a(\tau) d\tau, \lim_{\varepsilon \rightarrow 0} x_2 = a(t), \lim_{\varepsilon \rightarrow 0} x_3 = \dot{a}(t) \quad (23)$$

It can estimate the onefold integral and the first-order derivative of signal $a(t)$, respectively.

iv) Double integrator (where $n = 3$ and $p = 3$):

$$\begin{aligned} \dot{x}_1 &= x_2 \\ \dot{x}_2 &= x_3 \\ \varepsilon^4 \dot{x}_3 &= -k_1 \varepsilon x_1 - k_2 \varepsilon^2 x_2 - k_3 (x_3 - a(t)) \end{aligned} \quad (24)$$

where, $\varepsilon \in (0, 1)$; $k_1 > 0, k_3 > 0$ and $k_2 > \varepsilon^3 \frac{k_1}{k_3}$. The following conclusions hold:

$$\lim_{\varepsilon \rightarrow 0} x_1 = \int_0^t \int_0^\tau a(s) ds d\tau, \lim_{\varepsilon \rightarrow 0} x_2 = \int_0^t a(\tau) d\tau, \lim_{\varepsilon \rightarrow 0} x_3 = a(t) \quad (25)$$

It can estimate the onefold and double integrals of signal $a(t)$, respectively.

v) Differentiation and double-integration observer (where $n = 4$ and $p = 3$)

$$\begin{aligned} \dot{x}_1 &= x_2 \\ \dot{x}_2 &= x_3 \\ \dot{x}_3 &= x_4 \\ \varepsilon^5 \dot{x}_4 &= -k_1 \varepsilon x_1 - k_2 \varepsilon^2 x_3 - k_3 (x_3 - a(t)) - k_4 \varepsilon^4 x_4 \end{aligned} \quad (26)$$

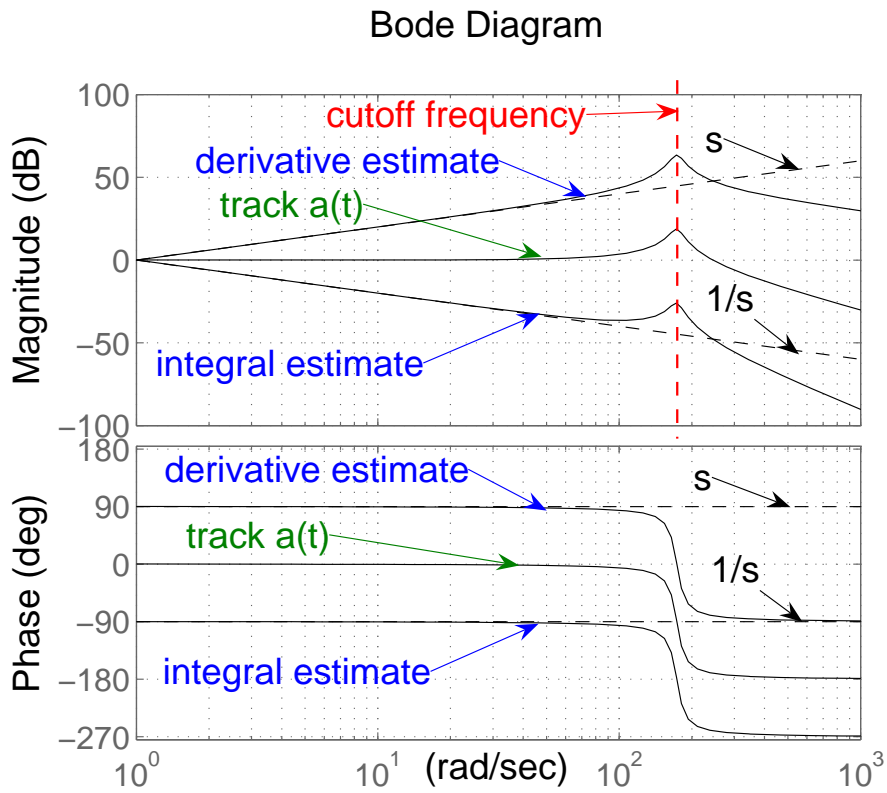
where, $\varepsilon \in (0, 1)$; $k_1 > 0, k_4 > 0, k_3 > \varepsilon^3 \frac{k_2}{k_4}$ and $k_2 > \varepsilon^3 \frac{k_4^2 k_1 + k_2^2}{k_4 k_3}$. The following conclusions hold:

$$\lim_{\varepsilon \rightarrow 0} x_1 = \int_0^t \int_0^\tau a(s) ds d\tau, \lim_{\varepsilon \rightarrow 0} x_2 = \int_0^t a(\tau) d\tau, \lim_{\varepsilon \rightarrow 0} x_3 = a(t), \lim_{\varepsilon \rightarrow 0} x_4 = \dot{a}(t), \quad (27)$$

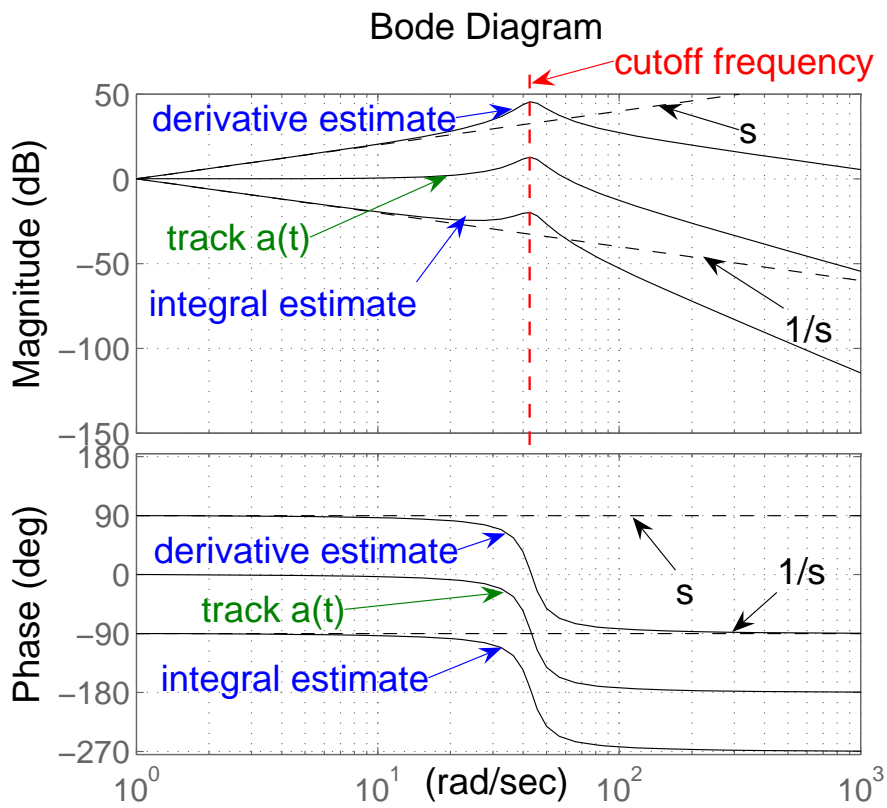
It can estimate the onefold, double integrals and the first-order derivative of signal $a(t)$, respectively.

3 Frequency analysis and parameters selection

In a practical problem, high-frequency noises exist in the measurement signal. The following analysis concerns the robustness behavior of the presented observers under high-frequency noise. We will adopt the Bode plots to analyze the frequency characteristics of the proposed differentiation-integration observers. Bode plots method is an indispensable component of the bag of tools of practicing control engineers. By the frequency analysis method, we can find that the presented differentiation-integration observers lead to perform rejection of high-frequency noise.

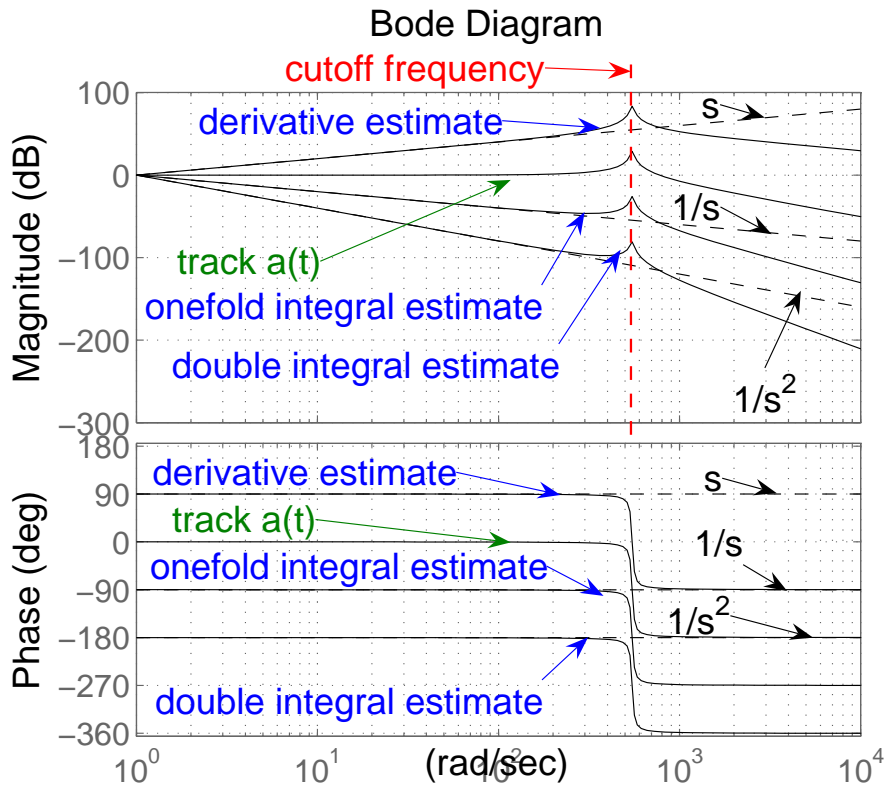


1(a) Bode plot when $\varepsilon = 0.1$

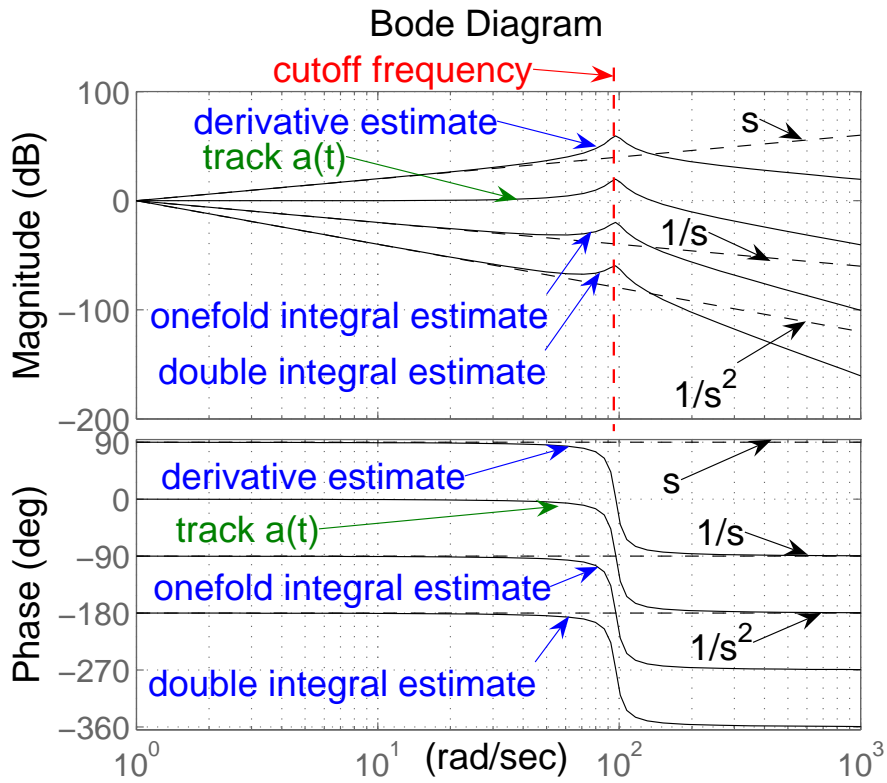


1(b) Bode plot when $\varepsilon = 0.2$

Figure 1 Bode plot of differentiation-integration observer



2(a) Bode plot when $\varepsilon = 0.1$



2(b) Bode plot when $\varepsilon = 0.2$

Figure 2 Bode plot of differentiation and double-integration observer

3.1 Frequency characteristic with different perturbation parameter ε

1) Differentiation-integration observer (22)

For transfer function (14), let $n = 3$, $p = 2$, we obtain

$$\frac{X_j(s)}{A(s)} = \frac{k_2 s^{j-1}}{\varepsilon^4 s^3 + \varepsilon^3 k_3 s^2 + k_2 s + \varepsilon k_1}, j \in \{1, 2, 3\} \quad (28)$$

where, $k_1 = 0.1$, $k_2 = 3$, $k_3 = 2$, Selecting $\varepsilon = 0.1$ and $\varepsilon = 0.2$, the Bode plots for the transfer function are described as Figs. 1(a) and 1(b), respectively.

2) Differentiation and double-integration observer (26)

For transfer function (14), let $n = 4$, $p = 3$, we obtain

$$\frac{X_j(s)}{A(s)} = \frac{k_3 s^{j-1}}{\varepsilon^5 s^4 + \varepsilon^4 k_4 s^3 + k_3 s^2 + \varepsilon^2 k_2 s + \varepsilon k_1}, j \in \{1, 2, 3, 4\} \quad (29)$$

where, $k_1 = 0.01$, $k_2 = 0.1$, $k_3 = 3$, $k_4 = 2$, Selecting $\varepsilon = 0.1$ and $\varepsilon = 0.2$, the Bode plots for the transfer function are described as Figs. 2(a) and 2(b), respectively.

Comparing with the ideal derivative operator s , the ideal integral operator $1/s$ and $1/s^2$, not only the presented differentiation-integration observers can obtain their estimations accurately, but also the high-frequency noise is rejected sufficiently (While in Figs. 1 and 2, the dash-lines represent the ideal operators and the solid lines represent the proposed observers). From Figs. 1 and 2, after the cutoff frequency lines, the estimations attenuate rapidly, and the high-frequency noises are also reduced sufficiently. Parameter ε affects the low-pass frequency bandwidth (See the cutoff frequency lines in Figures 1 and 2): Decreasing the perturbation parameter ε , the low-pass frequency bandwidth becomes larger, and the estimation speed becomes fast; on the other hand, increasing perturbation parameter ε , the low-pass frequency bandwidth becomes smaller, and much noise can be rejected sufficiently (See the cases of $\varepsilon = 0.1$ and $\varepsilon = 0.2$ in Figs.1 and 2, respectively).

3.2 The proposed rules of parameters selection

For the differentiation-integration observers, there are some rules suggested on the parameters selection:

1) The parameters k_i ($i = 1, \dots, n$) decide the observer stability, and they should be satisfied with the conditions in Lemma 1. Importantly, the selection of k_i ($i = 1, \dots, n$) should make the real parts of all the eigenvalues of polynomial (5) negative for the small $\varepsilon \in (0, 1)$.

a. For onefold integrator (20), the characteristic polynomial is $s^2 + \frac{k_2/\varepsilon^2}{\varepsilon} s + \frac{k_1}{\varepsilon^2}$ (See Eq. (16) when $n = 2$ and $p = 2$). In fact, for $\varepsilon \in (0, 1)$, the eigenvalues of the equivalent characteristic polynomial $s^2 + \frac{k_2}{\varepsilon^2} s + k_1$ (See Eq. (17) when $n = 2$ and $p = 2$) can be written as the following form: $-a_1, -a_2$ (The real eigenvalues of the characteristic polynomial for observer (20) are $-\frac{a_1}{\varepsilon}, -\frac{a_2}{\varepsilon}$). Therefore, this polynomial can be written as

$$s^2 + \frac{k_2}{\varepsilon^2} s + k_1 = (s + a_1)(s + a_2) = s^2 + (a_1 + a_2)s + a_1 a_2 \quad (30)$$

By solving the above equation, it follows that

$$k_1 = a_1 a_2, k_2 = \varepsilon^2 (a_1 + a_2)$$

From Eq. (14), the transfer function of the onefold integrator (20) can be described as

$$\frac{X_2(s)}{A(s)} = \frac{sk_2}{\varepsilon^3 s^2 + sk_2 + k_1 \varepsilon} = \frac{sk_2/\varepsilon^3}{s^2 + sk_2/\varepsilon^3 + k_1/\varepsilon^2} \quad (31)$$

Then its nature frequency is

$$\omega_n = \sqrt{k_1/\varepsilon^2} \quad (32)$$

Based on the requirement of filtering high-frequency noise, the perturbation parameter can be selected as

$$\varepsilon = \sqrt{k_1/\omega_n^2} \quad (33)$$

Because the drift is slow, the corresponding eigenvalue is selected to approach the imaginary axis with respect to the other eigenvalue. For example, let the eigenvalues be $-a_1 = -100$, $-a_2 = -0.02$, and select $\omega_n = 8$. Then we obtain the observer parameters as follows:

$$\begin{aligned} k_1 &= 100 \times 0.02 = 2 \\ \varepsilon &= 0.1768 \\ k_2 &= (100 + 0.02) \times (2/64) = 3.1256 \end{aligned}$$

b. For the double integrator (24) (when $n = 3$ and $p = 3$), the characteristic polynomial is $s^3 + \frac{k_3/\varepsilon^3}{\varepsilon} s^2 + \frac{k_2}{\varepsilon^2} s + \frac{k_1}{\varepsilon^3}$ (See Eq. (16) when $n = 3$ and $p = 3$). In fact, for $\varepsilon \in (0, 1)$, the eigenvalues of this equivalent characteristic polynomial $s^3 + \frac{k_3}{\varepsilon^3} s^2 + k_2 s + k_1$ (See Eq. (17) when $n = 3$ and $p = 3$) can be written as the following form: $-a_1$, $-a_{21} + a_{22}i$, $-a_{21} - a_{22}i$ (The real eigenvalues of the characteristic polynomial for observer (24) are $-\frac{a_1}{\varepsilon}$, $-\frac{a_{21}}{\varepsilon} + \frac{a_{22}}{\varepsilon}i$, $-\frac{a_{21}}{\varepsilon} - \frac{a_{22}}{\varepsilon}i$), where $a_1, a_{21}, a_{22} > 0$. Two conjugate eigenvalues are supposed to exist in this polynomial. Therefore, the polynomial $s^3 + \frac{k_3}{\varepsilon^3} s^2 + k_2 s + k_1$ can be written as

$$s^3 + \frac{k_3}{\varepsilon^3} s^2 + k_2 s + k_1 = (s + a_1)(s + a_{21} + a_{22}i)(s + a_{21} - a_{22}i) \quad (34)$$

By solving the above equation, it follows that

$$k_1 = a_1(a_{21}^2 + a_{22}^2), k_2 = a_{21}^2 + a_{22}^2 + 2a_1 a_{21}, k_3 = \varepsilon^3(a_1 + 2a_{21}) \quad (35)$$

It means that, after selecting the suitable eigenvalues $-a_1$, $-a_{21} + a_{22}i$, $-a_{21} - a_{22}i$ and ε based on Bode plot analysis, the parameters k_1 , k_2 and k_3 can be calculated. Because the drifts are slow, the corresponding eigenvalues are selected to approach the imaginary axis with respect to the other eigenvalues.

For example, selecting the eigenvalues of the polynomial as -46.8218 , $-0.0266+0.0999i$, $-0.0266-0.0999i$, and $\varepsilon = 0.4$, then $k_1 = 0.5$, $k_2 = 2.5$, $k_3 = 3$; selecting the eigenvalues as -15.6190 , $-0.0030 + 0.0800i$, $-0.0030 - 0.0800i$, and $\varepsilon = 0.4$, then $k_1 = 0.1$, $k_2 = 0.1$, $k_3 = 1$. Obviously, the first parameters selection has the stronger ability to correct the drift.

c. For differentiation-integration observer (22) (when $n = 3$ and $p = 2$), the characteristic polynomial is $s^3 + \frac{k_3}{\varepsilon}s^2 + \frac{k_2/\varepsilon^2}{\varepsilon^2}s + \frac{k_1}{\varepsilon^3}$ (See Eq. (16) when $n = 3$ and $p = 2$). In fact, for $\varepsilon \in (0, 1)$, the eigenvalues of the equivalent characteristic polynomial $s^3 + k_3s^2 + \frac{k_2}{\varepsilon^2}s + k_1$ (See Eq. (17) when $n = 3$ and $p = 2$) can be written as the following form: $-a_{11} + a_{12}i$, $-a_{11} - a_{12}i$, $-a_2$, (The real eigenvalues of the characteristic polynomial for observer (22) are $-\frac{a_{11}}{\varepsilon} + \frac{a_{12}}{\varepsilon}i$, $-\frac{a_{11}}{\varepsilon} - \frac{a_{12}}{\varepsilon}i$, $-\frac{a_2}{\varepsilon}$), where $a_{11}, a_{12}, a_1 > 0$. Two conjugate eigenvalues are supposed to exist in this polynomial. Therefore, the polynomial $s^3 + k_3s^2 + \frac{k_2}{\varepsilon^2}s + k_1$ can be written as

$$s^3 + k_3s^2 + \frac{k_2}{\varepsilon^2}s + k_1 = (s + a_{11} + a_{12}i)(s + a_{11} - a_{12}i)(s + a_2) \quad (36)$$

By solving the above equation, it follows that

$$k_1 = (a_{11}^2 + a_{12}^2)a_2, k_2 = \varepsilon^2(a_{11}^2 + a_{12}^2 + 2a_{11}a_2), k_3 = 2a_{11} + a_2 \quad (37)$$

It means that, after selecting the suitable eigenvalues $-a_{11} + a_{12}i$, $-a_{11} - a_{12}i$, $-a_2$ and ε based on Bode plot analysis, the parameters k_1 , k_2 and k_3 can be calculated.

2) In order to increase the estimation speed, $\varepsilon \in (0, 1)$ should decrease to make the low-pass frequency bandwidth larger; if much noise exists, ε should increase, the low-pass frequency bandwidth becomes smaller, and the noise can be rejected sufficiently.

3) It is easy to see that the k -fold integrator provides for a much better accuracy of i th-fold integral than the l -fold integrator, where, $k > l$ and $i = 1, \dots, l - 1$. For instance, the double integrator (24) provides for a much better accuracy of onefold integral than the onefold integrator (20).

4) It is easy to see that the k th-order differentiator provides for a much better accuracy of i th-order derivative than the l th-order differentiator, where, $k > l$ and $i = 1, \dots, l - 1$. For instance, in the high-order differentiator (18), the third-order differentiator (where $n = 3$) provides for a much better accuracy of first-order derivative than the second-order differentiator (where $n = 2$).

4 Estimations by onefold integrator and double integrator

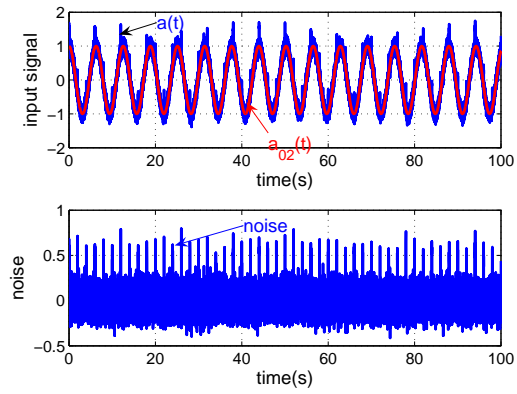
In this section, we use the simulations to illustrate the effectiveness of the proposed observers. The estimation performances of the presented observers are compared with Extended Kalman Filter (EKF) [23], and a long-time simulation is described to investigated their drift phenomena.

1) Estimation by onefold integrator (20)

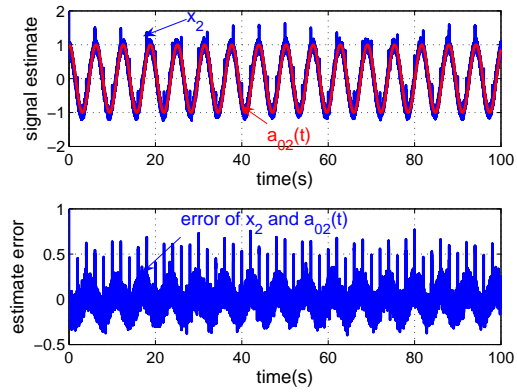
In this section, the onefold integrator (20), i.e.,

$$\begin{aligned} \dot{x}_1 &= x_2 \\ \varepsilon^3 \dot{x}_2 &= -k_1 \varepsilon x_1 - k_2 (x_2 - a(t)) \end{aligned}$$

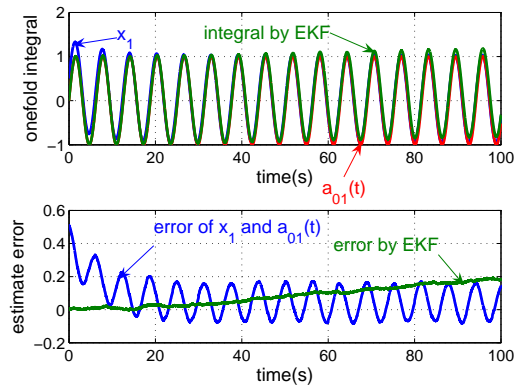
is used to estimate the integral from the signal $a(t)$ in spite of the existence of stochastic non-zero mean noise $\delta(t)$ and measurement error $d(t)$.



3(a) Input signal



3(b) Signal estimate



3(c) Onefold integral estimate

Figure 3 Estimation by onefold integrator (19) in 100s

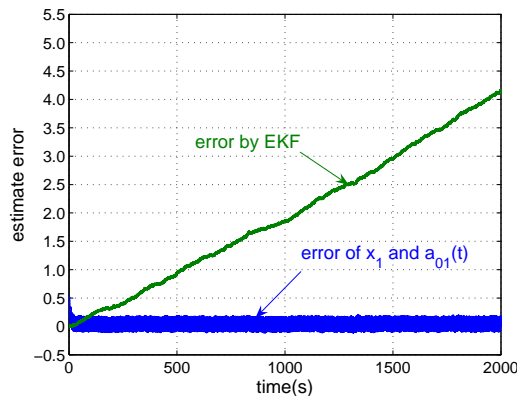
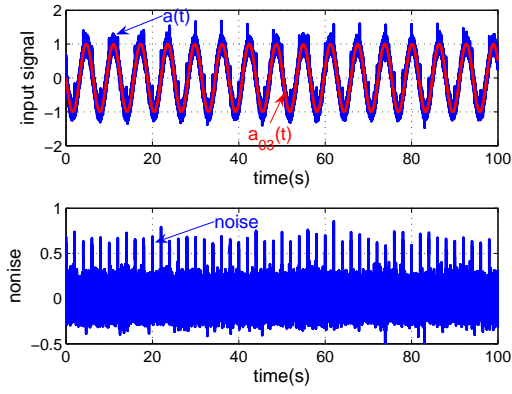
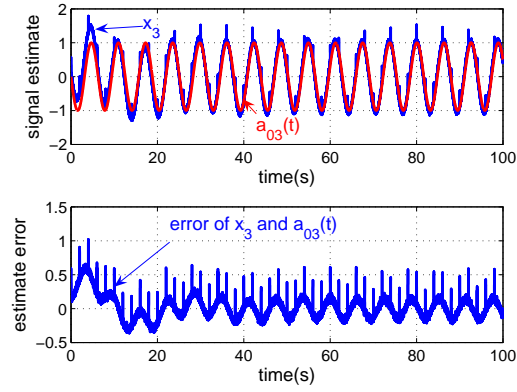


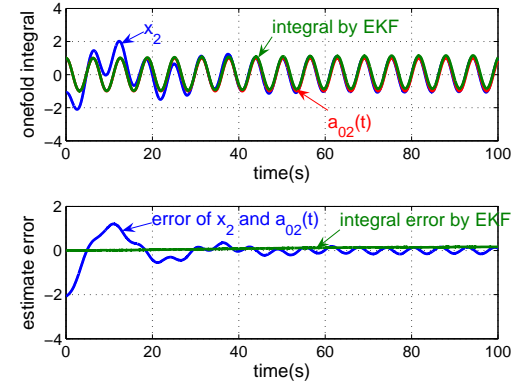
Figure 4 Comparison of onefold integrator (19) and EKF in 2000s



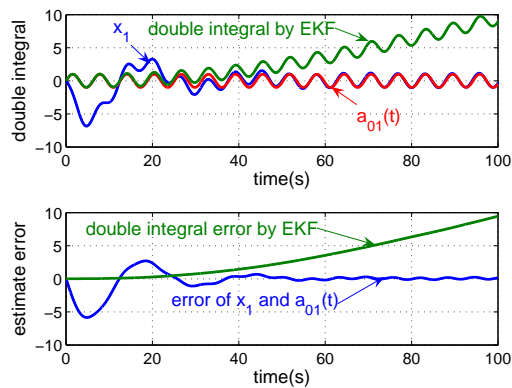
5(a) Input signal



5(b) Signal estimate

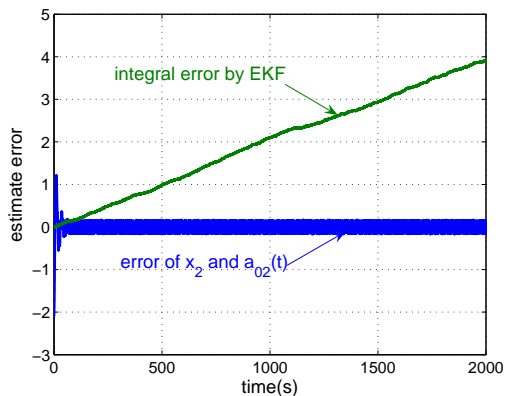


5(c) Onefold integral estimate

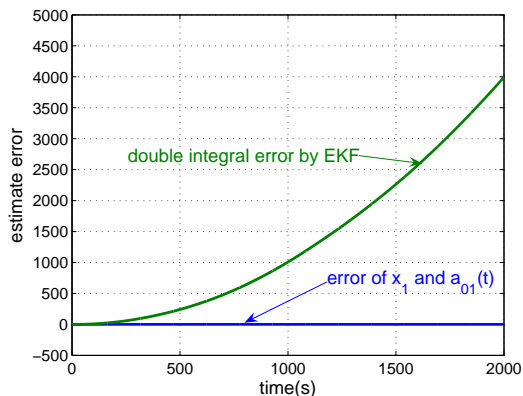


5(d) Double integral estimate

Figure 5 Estimation by double integrator (23) in 100s



6(a) Onefold integral estimate



6(a) Double integral estimate

6 Comparison of double integrator (23) and EKF in 2000s

Here, the stochastic non-zero mean noise is selected, and the mean value of the noise is not equal to zero (See the noise in Fig. 3(a)). The non-zero mean noise $\delta(t)$ consists of following two signals: Random number with Mean=0, Variance=0.01, Initial speed=0, and Sample time=0; Pulses with Amplitude=0.5, Period=2s, Pulse width=1, and Phase delay=0.

The signal $a_{02}(t) = \cos(t)$ is selected as the reference signal, and $a(t) = a_{02}(t) + \delta(t) + d(t)$. Therefore, $a_{01} = \int_0^t a(\tau) d\tau = \sin(t)$. Integrator parameters: $k_1 = 2$, $k_2 = 2.7783$, $\varepsilon = 0.1667$. Suppose the initial state is $(x_1(0), x_2(0)) = (0.5, 2)$. In the onefold integrator (20), x_2 estimates signal $a_{02}(t)$, x_1 estimate the onefold integral $a_{01}(t)$. Signal $a_{02}(t)$ tracking, the onefold integral estimation in 100 seconds are presented in Fig. 3. Fig. 3(a) provides signal $a_{02}(t)$ with stochastic noise. Fig. 3(b) describes signal $a_{02}(t)$ estimation. Fig. 3(c) presents the comparison of onefold integral estimation by onefold integrator (20) and Extended Kalman filter [23]. Figs. 4 describes the estimation comparison in 2000 seconds.

From Figs. 3(c) and 4, the obvious estimation drift of onefold integral exists by the Extended Kalman filter. With respect to the Extended Kalman filter, the proposed onefold integrator (20) showed the promising estimation ability and robustness in spite of the existence of the non-zero mean stochastic noise. Furthermore, from Fig. 4, no drift phenomenon happened in the long-time estimation.

2) Estimation by double integrator (24)

In this section, the double integrator (24), i.e.,

$$\begin{aligned}\dot{x}_1 &= x_2 \\ \dot{x}_2 &= x_3 \\ \varepsilon^4 \dot{x}_3 &= -k_1 \varepsilon x_1 - k_2 \varepsilon^2 x_2 - k_3 (x_3 - a(t))\end{aligned}$$

is used to estimate the onefold and double integrals from the signal $a(t)$ in spite of the existence of stochastic non-zero mean noise $\delta(t)$ and measurement error $d(t)$.

Here, the stochastic non-zero mean noise in 1) is selected.

The signal $a_{03}(t) = -\sin(t)$ is selected as the reference signal, and $a(t) = a_{03}(t) + \delta(t) + d(t)$. Therefore, $a_{02} = \int_0^t a_{03}(\sigma) d\sigma = \cos(t)$, and $a_{01} = \int_0^t \int_0^s a(\sigma) d\sigma d\tau = \sin(t)$.

The double integrator parameters: $k_1 = 0.5$, $k_2 = 2.5$, $k_3 = 3$, $\varepsilon = 0.4$. Suppose the initial state is $(x_1(0), x_2(0), x_3(0)) = (0.1, -1.1, 0.1)$. In the double integrator (24), x_3 tracks signal $a_{03}(t)$, x_2 and x_1 estimate the onefold and double integrals of signal $a_{03}(t)$, respectively.

Signal $a_{03}(t)$ tracking, the onefold and double integral estimations in 100 seconds are presented in Fig. 5. Fig. 5(a) provides signal $a_{03}(t)$ with stochastic noise. Fig. 5(b) describes $a_{03}(t)$ estimation. Figs. 5(c) and 5(d) present the comparisons of onefold and double integral estimations by the double integrator (24) and the Extended Kalman filter [23]. Figs. 6(a)-6(b) describe the estimation comparisons of in 2000 seconds.

From Figs. 5(c), 5(d), 6(a) and 6(b), the obvious estimation drifts of onefold and double integrals exist by the Extended Kalman filter. With respect to the Extended Kalman filter, despite the existence of the intensive non-zero mean stochastic noise, the proposed double integrator (24) showed the promising estimation ability and robustness. Furthermore, from Figs. 6(a)-6(b), no drift phenomenon happened in the long-time estimations.

5 Application to quadrotor aircraft

In this paper, the mathematical model and reference trajectory of the quadrotor aircraft described in [29] are used. The description of forces and torques of the quadrotor aircraft is shown in Fig. 7 [29].

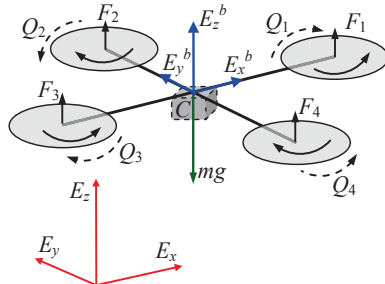


Figure 7 Forces and torques of quadrotor aircraft

Let $\Xi_g = (E_x, E_y, E_z)$ denote the right handed inertial frame, and $\Xi_b = (E_x^b, E_y^b, E_z^b)$ denote the frame attached to the aircraft's fuselage whose origin is at the center of gravity. (ψ, θ, ϕ) denotes the aircraft orientation expressed in the yaw, pitch and roll angles (Euler angles). The symbol c_θ is used for $\cos \theta$ and s_θ for $\sin \theta$. R_{bg} is the transformation matrix from the frame Ξ_b to Ξ_g , and

$$R_{bg} = \begin{bmatrix} c_\psi c_\theta & s_\psi c_\phi + c_\psi s_\theta s_\phi & s_\psi s_\phi - c_\psi s_\theta c_\phi \\ -s_\psi c_\theta & c_\psi c_\phi - s_\psi s_\theta s_\phi & c_\psi s_\phi + s_\psi s_\theta c_\phi \\ s_\theta & -c_\theta s_\phi & c_\theta c_\phi \end{bmatrix} \quad (38)$$

For the quadrotor aircraft, the right-left rotors rotate clockwise and the front-rear ones rotate counterclockwise (See Fig. 7). The rotational directions of the rotors do not change (i.e., $\omega_i > 0$, $i \in \{1, 2, 3, 4\}$). The reactive torque generated by the rotor i due to the rotor drag is $Q_i = k\omega_i^2$, and the total thrust generated by the four rotors is $F = \sum_{i=1}^4 F_i = b \sum_{i=1}^4 \omega_i^2$, where $F_i = b\omega_i^2$ is the lift generated by the rotor i in free air, and $k, b > 0$ are two parameters depending on the density of air, the size, shape, and pitch angle of the blades, as well as other factors. Therefore, we obtain $Q_i = \frac{k}{b}F_i, i = 1, 2, 3, 4$. Thus the sum reactive torque generated by the four rotors due to the rotor drags is $Q = \sum_{i=1}^4 (-1)^i Q_i = \frac{k}{b} \sum_{i=1}^4 (-1)^i F_i$.

The motion equations in the coordinate (x, y, z) are then [29]

$$\begin{aligned} m\ddot{x} &= (s_\psi s_\phi - c_\psi s_\theta c_\phi)F - k_x \dot{x} + \delta_x \\ m\ddot{y} &= (c_\psi s_\phi + s_\psi s_\theta c_\phi)F - k_y \dot{y} + \delta_y \\ m\ddot{z} &= c_\theta c_\phi F - mg - k_z \dot{z} + \delta_z \end{aligned} \quad (39)$$

$$\begin{aligned} J_z \ddot{\psi} &= \frac{k}{b} \sum_{i=1}^4 (-1)^i F_i - k_\psi \dot{\psi} + \delta_\psi \\ J_y \ddot{\theta} &= (F_1 - F_3)l - lk_\theta \dot{\theta} + \delta_\theta \\ J_x \ddot{\phi} &= (F_2 - F_4)l - lk_\phi \dot{\phi} + \delta_\phi \end{aligned} \quad (40)$$

where, m is the mass of the aircraft; g is the gravity acceleration; J_x, J_y and J_z are the three-axis moment of inertias; $k_x, k_y, k_z, k_\psi, k_\theta$ and k_ϕ are the drag coefficients; l is the distance between each rotor and the center of gravity. δ_x, δ_y and δ_z are the bounded disturbances and uncertainties in position dynamics; $\delta_\psi, \delta_\theta$ and δ_ϕ are the bounded disturbances and uncertainties in attitude dynamics.

Here, for the quadrotor aircraft, we are interested in designing the observers to estimate $(\dot{x}, \dot{y}, \dot{z}, \psi, \theta, \phi)$ and the uncertainties $(k_x, k_y, k_z, k_\psi, k_\theta, k_\phi)$ and $(\delta_x, \delta_y, \delta_z, \delta_\psi, \delta_\theta, \delta_\phi)$ from the information of $(x, y, z, \dot{\psi}, \dot{\theta}, \dot{\phi})$. Moreover, based on these observers, the controllers F_i ($i = 1, 2, 3, 4$) will be designed to implement: $x \rightarrow x_d, \dot{x} \rightarrow \dot{x}_d, y \rightarrow y_d, \dot{y} \rightarrow \dot{y}_d, z \rightarrow z_d, \dot{z} \rightarrow \dot{z}_d$, and $\psi \rightarrow \psi_d, \dot{\psi} \rightarrow \dot{\psi}_d, \theta \rightarrow \theta_d, \dot{\theta} \rightarrow \dot{\theta}_d, \phi \rightarrow \phi_d, \dot{\phi} \rightarrow \dot{\phi}_d$ as $t \rightarrow \infty$.

4.1 Observer designs for the quadrotor aircraft

For quadrotor aircraft equations (39) and (40), we consider that $(\dot{x}, \dot{y}, \dot{z}, \psi, \theta, \phi)$ is not measured

directly, $(k_x, k_y, k_z, k_\psi, k_\theta, k_\phi)$ and $(\delta_x, \delta_y, \delta_z, \delta_\psi, \delta_\theta, \delta_\phi)$ are bounded and unknown. Select the auxiliary controller vector as

$$u_p = \begin{bmatrix} u_{px} \\ u_{py} \\ u_{pz} \end{bmatrix} = \begin{bmatrix} s_\psi s_\phi - c_\psi s_\theta c_\phi \\ c_\psi s_\phi + s_\psi s_\theta c_\phi \\ c_\theta c_\phi \end{bmatrix} F \quad (41)$$

Then we can find that

$$F = \|u_p\|_2 = \sqrt{u_{px}^2 + u_{py}^2 + u_{pz}^2} \quad (42)$$

That is to say, after designing (u_{px}, u_{py}, u_{pz}) , F can be calculated. Therefore, (u_{px}, u_{py}, u_{pz}) is known. Let [29]

$$\begin{aligned} h_1(t) &= \frac{u_{px}}{m}, h_2(t) = \frac{u_{py}}{m}, h_3(t) = \frac{u_{pz}}{m} - g, \\ h_4(t) &= \frac{k}{J_z b} \sum_{i=1}^4 (-1)^i F_i, h_5(t) = \frac{l}{J_y} (F_1 - F_3), h_6(t) = \frac{l}{J_x} (F_2 - F_4) \end{aligned} \quad (43)$$

$$\begin{aligned} d_1(t) &= (\delta_x - k_x \dot{x})/m, d_2(t) = (\delta_y - k_y \dot{y})/m, \\ d_3(t) &= (\delta_z - k_z \dot{z})/m, d_4(t) = (\delta_\psi - k_\psi \dot{\psi})/J_z, \\ d_5(t) &= (\delta_\theta - l k_\theta \dot{\theta})/J_y, d_6(t) = (\delta_\phi - l k_\phi \dot{\phi})/J_x \end{aligned} \quad (44)$$

$$\begin{aligned} w_{1,1} &= x, w_{2,1} = y, w_{3,1} = z, w_{4,1} = \psi, w_{5,1} = \theta, w_{6,1} = \phi \\ w_{1,2} &= \dot{x}, w_{2,2} = \dot{y}, w_{3,2} = \dot{z}, w_{4,2} = \dot{\psi}, w_{5,2} = \dot{\theta}, w_{6,2} = \dot{\phi} \end{aligned} \quad (45)$$

then the position dynamics (39) can be rewritten as

$$\begin{aligned} \dot{w}_{i,1} &= w_{i,2} \\ \dot{w}_{i,2} &= h_i(t) + d_i(t) \\ y_{opi} &= w_{i,1} \end{aligned} \quad (46)$$

where $i = 1, 2, 3$, and the attitude dynamics (40) can be given by

$$\begin{aligned} \dot{w}_{i,1} &= w_{i,2} \\ \dot{w}_{i,2} &= h_i(t) + d_i(t) \\ y_{opi} &= w_{i,2} \end{aligned} \quad (47)$$

where $i = 4, 5, 6$.

Based on Theorem 1 and Lemma 1, the following corollaries describe the the observer designs for the quadrotor aircraft.

1) *The third-order differentiator (18) for velocity and uncertainties estimate in position dynamics*

The following corollary gives the observers to estimate $(\dot{x}, \dot{y}, \dot{z})$ and uncertainties in the position dynamics.

Corollary 2: The observer (18) (where $n = 3$) are designed for aircraft position dynamics (39) as follows:

$$\begin{aligned}\dot{x}_{i,1} &= x_{i,2} \\ \dot{x}_{i,2} &= x_{i,3} \\ \varepsilon_i^3 \dot{x}_{i,3} &= -k_1(x_{i,1} - w_{i,1}) - k_2 \varepsilon_i x_{i,2} - k_3 \varepsilon_i^2 x_{i,3}\end{aligned}\quad (48)$$

where $i = 1, 2, 3$. From (x, y, z) , we can estimate $(\dot{x}, \dot{y}, \dot{z})$ and $d_i(t)$ ($i = 1, 2, 3$) by the differentiators in Eq. (48), and the following conclusions hold:

$$\begin{aligned}\lim_{\varepsilon \rightarrow 0} x_{1,1} &= x, \lim_{\varepsilon \rightarrow 0} x_{1,2} = \dot{x}, \lim_{\varepsilon \rightarrow 0} x_{1,3} - h_1(t) = d_1(t) \\ \lim_{\varepsilon \rightarrow 0} x_{2,1} &= y, \lim_{\varepsilon \rightarrow 0} x_{2,2} = \dot{y}, \lim_{\varepsilon \rightarrow 0} x_{2,3} - h_2(t) = d_2(t) \\ \lim_{\varepsilon \rightarrow 0} x_{3,1} &= z, \lim_{\varepsilon \rightarrow 0} x_{3,2} = \dot{z}, \lim_{\varepsilon \rightarrow 0} x_{3,3} - h_3(t) = d_3(t)\end{aligned}\quad (49)$$

2) *Differentiation-integration observer (22) for attitude angle estimation*

The following corollary gives the observers to estimate (ψ, θ, ϕ) and uncertainties in the attitude dynamics.

Corollary 3: The differentiation-integrator observers are designed for aircraft attitude dynamics (40) as follows:

$$\begin{aligned}\dot{x}_{i,1} &= x_{i,2} \\ \dot{x}_{i,2} &= x_{i,3} \\ \varepsilon_i^4 \dot{x}_{i,3} &= -k_{i,1} \varepsilon_i x_{i,1} - k_{i,2}(x_{i,2} - w_{i,2}) - k_{i,3} \varepsilon_i^3 x_{i,3}\end{aligned}\quad (50)$$

where $i = 4, 5, 6$. From $(\dot{\psi}, \dot{\theta}, \dot{\phi})$, we can estimate (ψ, θ, ϕ) and $d_i(t)$ ($i = 4, 5, 6$) by the differentiation-integration observers in Eq. (50), and the following conclusions hold:

$$\begin{aligned}\lim_{\varepsilon \rightarrow 0} x_{4,1} &= \psi, \lim_{\varepsilon \rightarrow 0} x_{4,2} = \dot{\psi}, \lim_{\varepsilon \rightarrow 0} x_{4,3} - h_4(t) = d_4(t) \\ \lim_{\varepsilon \rightarrow 0} x_{5,1} &= \theta, \lim_{\varepsilon \rightarrow 0} x_{5,2} = \dot{\theta}, \lim_{\varepsilon \rightarrow 0} x_{5,3} - h_5(t) = d_5(t) \\ \lim_{\varepsilon \rightarrow 0} x_{6,1} &= \phi, \lim_{\varepsilon \rightarrow 0} x_{6,2} = \dot{\phi}, \lim_{\varepsilon \rightarrow 0} x_{6,3} - h_6(t) = d_6(t)\end{aligned}\quad (51)$$

4.2 Controller design

In this section, a control law will be designed for the attitude stabilization and trajectory tracking. The unknown states and uncertainties are reconstructed by the presented observers. Suppose the reference trajectory and its finite-order derivatives are bounded, and they can be generated directly.

For reference trajectory (x_d, y_d, z_d) , define $e_1 = x - x_d$, $e_2 = \dot{x} - \dot{x}_d$, $e_3 = y - y_d$, $e_4 = \dot{y} - \dot{y}_d$, $e_5 = z - z_d$, and $e_6 = \dot{z} - \dot{z}_d$. The system error for position dynamics (39) can be written as

$$\ddot{e}_p = m^{-1}(u_p + \Xi_p + \delta_p) \quad (52)$$

where

$$e_p = [e_1 \ e_3 \ e_5]^T, \Xi_p = \begin{bmatrix} -m\ddot{x}_d \\ -m\ddot{y}_d \\ -m\ddot{z}_d - mg \end{bmatrix}, \delta_p = \begin{bmatrix} \delta_x - k_x \dot{x} \\ \delta_y - k_y \dot{y} \\ \delta_z - k_z \dot{z} \end{bmatrix} \quad (53)$$

For reference attitude angle $(\psi_d, \theta_d, \phi_d)$, define $e_7 = \psi - \psi_d$, $e_8 = \dot{\psi} - \dot{\psi}_d$, $e_9 = \theta - \theta_d$, $e_{10} = \dot{\theta} - \dot{\theta}_d$, $e_{11} = \phi - \phi_d$, $e_{12} = \dot{\phi} - \dot{\phi}_d$. The system error for attitude dynamics (40) is given by

$$\ddot{e}_a = J^{-1}(u_a + \Xi_a + \delta_a) \quad (54)$$

where

$$e_a = \begin{bmatrix} e_7 \\ e_9 \\ e_{11} \end{bmatrix}, u_a = \begin{bmatrix} \frac{k}{b} \sum_{i=1}^4 (-1)^i F_i \\ (F_1 - F_3)l \\ (F_2 - F_4)l \end{bmatrix}, \Xi_a = \begin{bmatrix} -J_z \ddot{\psi}_d \\ -J_y \ddot{\theta}_d \\ -J_x \ddot{\phi}_d \end{bmatrix}, \delta_a = \begin{bmatrix} \delta_\psi - k_\psi \dot{\psi} \\ \delta_\theta - lk_\theta \dot{\theta} \\ \delta_\phi - lk_\phi \dot{\phi} \end{bmatrix}, J = \text{diag}\{J_z, J_y, J_x\} \quad (55)$$

4.2.1 Controller design for position dynamics

Theorem 2: For the position dynamics (39), to track the reference trajectory (x_d, y_d, z_d) , if the controller is selected as

$$u_p = -\Xi_p - \hat{\delta}_p - m(k_{p1}\hat{e}_p + k_{p2}\dot{\hat{e}}_p) \quad (56)$$

where $\hat{e}_1 = \hat{x} - x_d$, $\hat{e}_2 = \hat{\dot{x}} - \dot{x}_d$, $\hat{e}_3 = \hat{y} - y_d$, $\hat{e}_4 = \hat{\dot{y}} - \dot{y}_d$, $\hat{e}_5 = \hat{z} - z_d$, $\hat{e}_6 = \hat{\dot{z}} - \dot{z}_d$; $k_{p1}, k_{p2} > 0$, and

$$\hat{e}_p = \begin{bmatrix} \hat{e}_1 \\ \hat{e}_3 \\ \hat{e}_5 \end{bmatrix}, \dot{\hat{e}}_p = \begin{bmatrix} \hat{e}_2 \\ \hat{e}_4 \\ \hat{e}_6 \end{bmatrix}, \hat{\delta}_p = \begin{bmatrix} x_{1,3} \\ x_{2,3} \\ x_{3,3} \end{bmatrix} \quad (57)$$

then the position error dynamics (52) rendering by controller (56) will converge asymptotically to the origin, i.e., the tracking errors $e_p \rightarrow 0$ and $\dot{e}_p \rightarrow 0$ as $t \rightarrow \infty$.

The proof of Theorem 2 is presented in Appendix.

From (41), (42) and (56), we obtain

$$F = \left\| -\Xi_p - \hat{\delta}_p - m(k_{p1}\hat{e}_p + k_{p2}\dot{\hat{e}}_p) \right\|_2 \quad (58)$$

4.2.2 Controller design for attitude dynamics

Theorem 3: For the attitude dynamics (40), to track the reference attitude $(\psi_d, \theta_d, \phi_d)$, if the controller is selected as

$$u_a = -\Xi_a - \hat{\delta}_a - J(k_{a1}\hat{e}_a + k_{a2}\dot{\hat{e}}_a) \quad (59)$$

where $\hat{e}_7 = \hat{\psi} - \psi_d$, $\hat{e}_8 = \hat{\psi} - \dot{\psi}_d$, $\hat{e}_9 = \hat{\theta} - \theta_d$, $\hat{e}_{10} = \hat{\theta} - \dot{\theta}_d$, $\hat{e}_{11} = \hat{\phi} - \phi_d$, $\hat{e}_{12} = \hat{\phi} - \dot{\phi}_d$; $k_{a1}, k_{a2} > 0$, and

$$\hat{e}_a = \begin{bmatrix} \hat{e}_7 \\ \hat{e}_9 \\ \hat{e}_{11} \end{bmatrix}, \hat{e}_a = \begin{bmatrix} \hat{e}_8 \\ \hat{e}_{10} \\ \hat{e}_{12} \end{bmatrix}, \hat{\delta}_a = \begin{bmatrix} x_{4,3} \\ x_{5,3} \\ x_{6,3} \end{bmatrix} \quad (60)$$

then the attitude error dynamics (54) rendering by controller (59) will converge asymptotically to the origin, i.e., the tracking errors $e_a \rightarrow 0$ and $\dot{e}_a \rightarrow 0$ as $t \rightarrow \infty$.

The proof of Theorem 3 is presented in Appendix.

4.3 Computational analysis and simulation on quadrotor aircraft

In this section, we use a simulation on a quadrotor aircraft to illustrate the effectiveness of the proposed estimate and control methods. When the quadrotor desired attitude is calculated to track the translational trajectories, the under-actuated dynamics nature exists. Here, only the performance of the proposed observers are validated, and the reference trajectory is selected to make the desired attitude satisfy $(\psi_d, \theta_d, \phi_d) = (0, 0, 0)$. The goal is to force the aircraft to track a reference trajectory in the vertical direction. Here, the quadrotor aircraft tracks a given trajectory (x_d, y_d, z_d) without the information of $(\dot{x}, \dot{y}, \dot{z}, \psi, \theta, \phi, d_1, d_2, d_3, d_4, d_5, d_6)$.

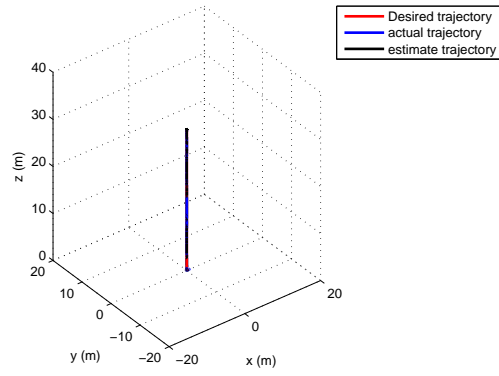
The observers (48) and (50) are used to estimate $(\dot{x}, \dot{y}, \dot{z}, \psi, \theta, \phi, d_1, d_2, d_3, d_4, d_5, d_6)$ from the measurements of position (x, y, z) and the angular velocity $(\dot{\psi}, \dot{\theta}, \dot{\phi})$. The controllers (56) and (59) are presented to stabilize the flight dynamics. On the other hand, the estimation performances by the observer (50) are compared with those by the Extended Kalman filter [23].

Here, the aircraft is driven to move from $(0, 0, 0)$ to $(0, 0, h_z)$. The reference trajectory is arranged as the following expression [29]:

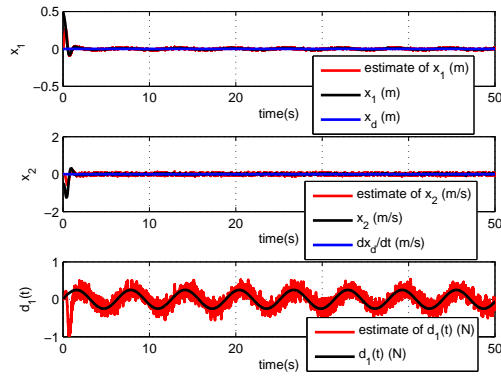
$$x_d = 0, \dot{x}_d = 0, \ddot{x}_d = 0; y_d = 0, \dot{y}_d = 0, \ddot{y}_d = 0;$$

$$z_d = h_0(1 - e^{-0.5k_m at^2}), \dot{z}_d = h_0 k_m a t e^{-0.5k_m at^2}, \ddot{z}_d = h_0 k_m a (1 - k_m at^2) e^{-0.5k_m at^2}$$

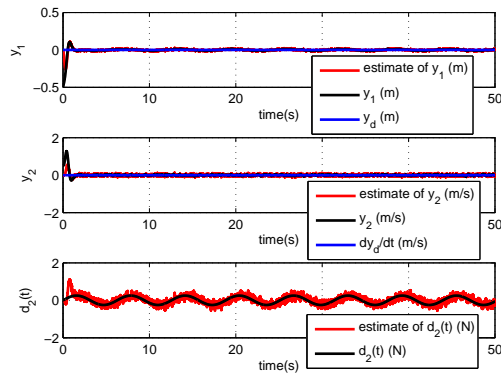
The initial states of quadrotor aircraft are: $(x(0), \dot{x}(0), y(0), \dot{y}(0), z(0), \dot{z}(0), \psi(0), \dot{\psi}(0), \theta(0), \dot{\theta}(0), \phi(0), \dot{\phi}(0)) = (0.5, -0.5, -0.5, 0.5, 0.5, -1, 0.2, 0.3, 0.3, -0.1, 0.2, -0.2)$; the initial states of the observers are: $(x_{1,1}(0), x_{1,2}(0), x_{1,3}(0), x_{2,1}(0), x_{2,2}(0), x_{2,3}(0), x_{3,1}(0), x_{3,2}(0), x_{3,3}(0), x_{4,1}(0), x_{4,2}(0), x_{4,3}(0), x_{5,1}(0), x_{5,2}(0), x_{5,3}(0), x_{6,1}(0), x_{6,2}(0), x_{6,3}(0)) = (0, 0, 0, 0, 0, 0, 0, 0, 0, 0, 0.2, 0.3, 0, 0.3, -0.1, 0, 0.2, -0.2, 0)$. Let the uncertainties be: $\delta_x = 0.5 \sin(t)$, $\delta_y = 0.5 \sin(t)$, $\delta_z = 0.5 \sin(t)$, $\delta_\psi = 0.2 \sin(0.8t)$, $\delta_\theta = 0.2 \sin(0.8t)$, $\delta_\phi = 0.2 \sin(0.8t)$.



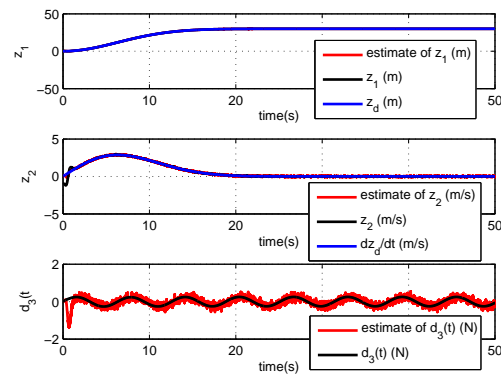
8(a) Position trajectory



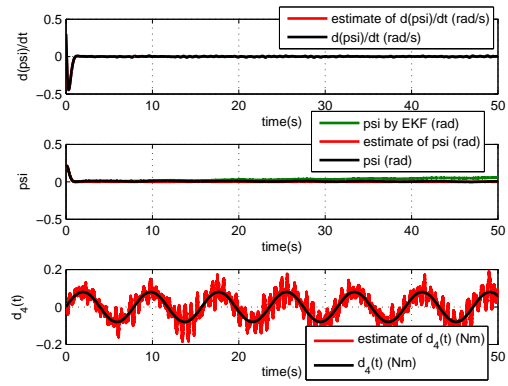
8(b) Estimation in x coordinate



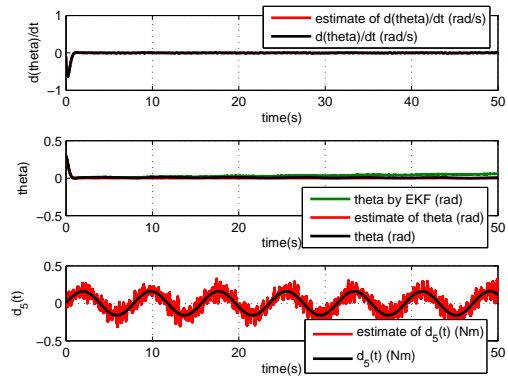
8(c) Estimation in y coordinate



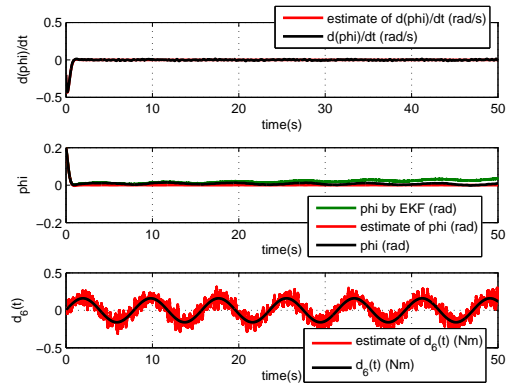
8(d) Estimation in z coordinate



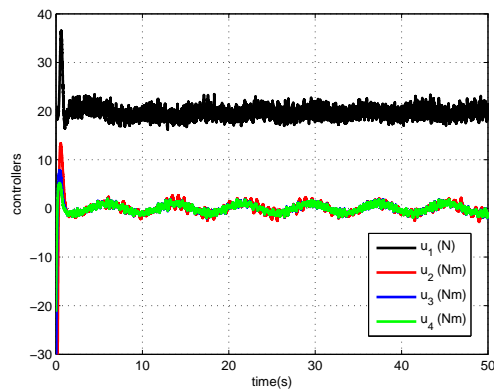
8(e) Estimation in yaw dynamics



8(f) Estimation in pitch dynamics

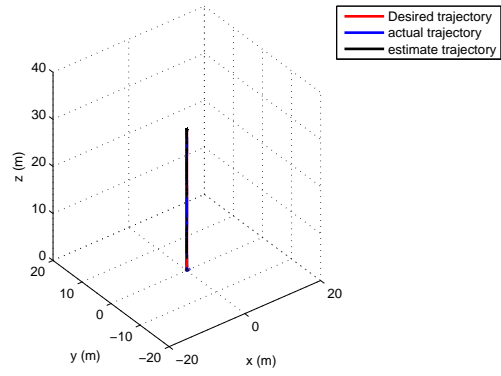


8(g) Estimation in roll dynamics

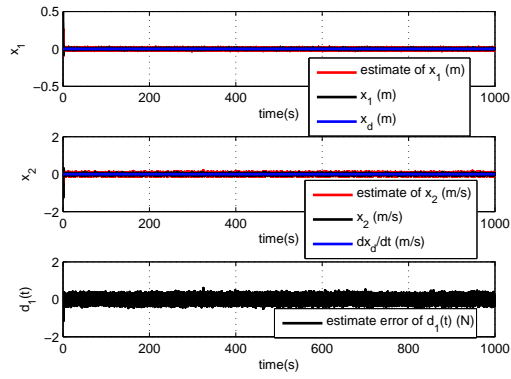


8(h) Controller

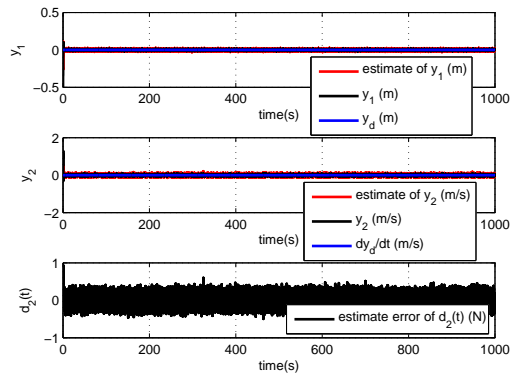
Figure 8 Quadrotor aircraft control based on differentiation-integration observer in 50s



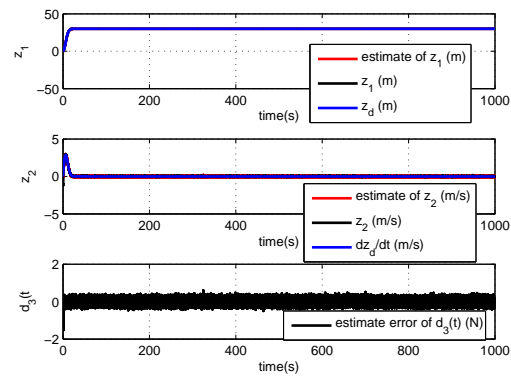
9(a) Position trajectory



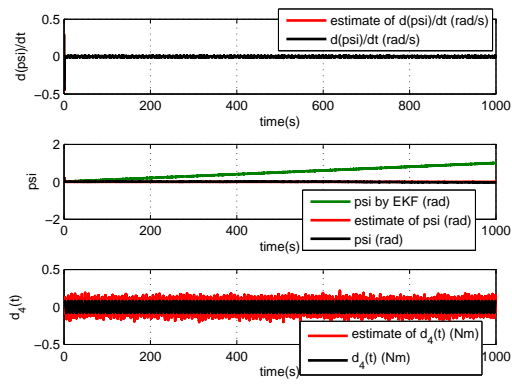
9(b) Estimation in x coordinate



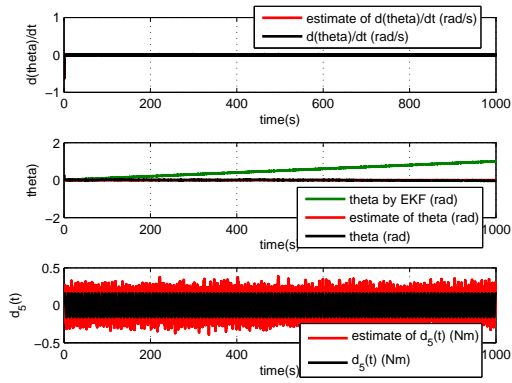
9(c) Estimation in y coordinate



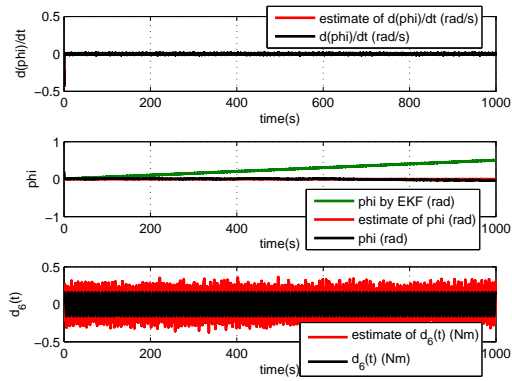
9(d) Estimation in z coordinate



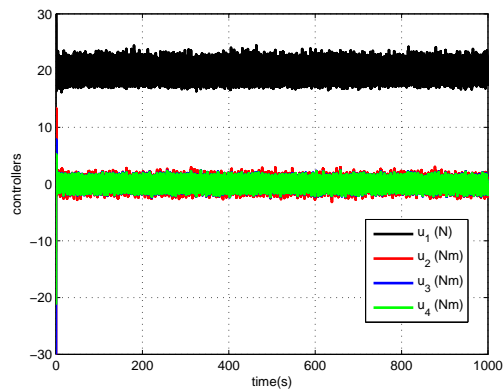
9(e) Estimation in yaw dynamics



9(f) Estimation in pitch dynamics



9(g) Estimation in roll dynamics



9(h) Controller

Figure 9 Quadrotor aircraft control based on differentiation-integration observer in 1000s

The position measurement outputs are $y_{opi} = w_{i,1} + n_i$, where $i = 1, 2, 3$, and $w_{1,1} = x$, $w_{2,1} = y$, $w_{3,1} = z$; the attitude measurement outputs are $y_{opi} = w_{i,2} + n_i$, where $i = 4, 5, 6$, and $w_{4,2} = \dot{\psi}$, $w_{5,2} = \dot{\theta}$, $w_{6,2} = \dot{\phi}$; n_i (where $i = 1, \dots, 6$) are the disturbances.

The disturbances n_i (where $i = 1, \dots, 6$) include two types of noises: Random number with Mean=0, Variance=0.001, Initial speed=0, and Sample time=0; Pulses with Amplitude=0.001, Period=1s, Pulse width=1, and Phase delay=0.

The parameters of the aircraft control system are given as follows:

Quadrotor aircraft [29]: $m = 2kg$, $g = 9.81m/s^2$, $l = 0.2m$, $J_x = 1.25Ns^2/rad$, $J_y = 1.25Ns^2/rad$, $J_z = 2.5Nm$; $b = 2.923 \times 10^{-3}$, $k = 5 \times 10^{-4}$, $k_x = k_y = k_z = 0.01Ns/m$, $k_\psi = k_\theta = k_\phi = 0.012Ns/rad$;

Third-order differentiator: $k_{i,1} = 6$, $k_{i,2} = 11$, $k_{i,3} = 6$, $i = 1, 2, 3$;

In order to reduce the peaking phenomena in the outputs of the differentiator due to the large initial observation errors, the perturbation parameters are selected as $1/\varepsilon_i = \begin{cases} 5t, t \leq 1 \\ 5, t > 1 \end{cases}$, $i = 1, 2, 3$;

Differentiation-integration observer: $k_{2,i,1} = 0.1$, $k_{2,i,2} = 2$, $k_{2,i,3} = 1$, $i = 4, 5, 6$;

Because the initial observation errors are small for the differentiation-integration observer, no chattering phenomenon happen, and the perturbation parameter can be selected as $\varepsilon_i = 1/3$, $i = 4, 5, 6$;

Reference trajectory: $h_0 = 30m$, $a = 5m/s^2$, $k_m = 0.005$;

Controllers: $k_{p1} = 16$, $k_{p2} = 8$, $k_{a1} = 28$, $k_{a2} = 8$.

In this simulation, without the information of velocity, attitude angle and uncertainties, the aircraft is controlled to track the reference trajectory. The position is obtained from the GPS receiver, and the altitude information is from the altimeter. The angular velocity $(\dot{\psi}, \dot{\theta}, \dot{\phi})$ is measured by the IMU. Differentiation-integration observer (50) is used to estimate the attitude angle (ψ, θ, ϕ) and uncertainties in the attitude dynamics from measurement of the angular velocity $(\dot{\psi}, \dot{\theta}, \dot{\phi})$. The third-order differentiator (48) is adopted to estimate the velocity $(\dot{x}, \dot{y}, \dot{z})$ and uncertainties in the position dynamics from the measurement of position (x, y, z) . Controllers (56) and (59) are designed to control the aircraft to track the reference trajectory.

The data of flying test are presented in Figs.8 and 9. Fig. 8(a) describes the position trajectory; Fig. 8(b) describes the estimate of x , dx/dt and $d_1(t)$; Fig. 8(c) describes the estimate of y , dy/dt and $d_2(t)$; Fig. 8(d) presents the estimate of z , dz/dt and $d_3(t)$; Fig. 8(e) presents the estimate of the yaw angle ψ , yaw rate $d\psi/dt$ and $d_4(t)$; Fig. 8(f) presents the estimate of the pitch angle θ , pitch rate $d\theta/dt$ and $d_5(t)$; Fig. 8(g) presents the estimate of the roll angle ϕ , roll rate $d\phi/dt$ and $d_1(t)$; Fig. 8(h) presents the controller curves of u_1 , u_2 , u_3 and u_4 . The simulation in 1000s is proposed in Fig. 9. In the simulation above, though high-frequency stochastic noises exist in the measurement signals, the uncertainties exist in the aircraft dynamics, and only the angular velocity is considered in the IMU output, the attitude estimations by the presented differentiation-integration observer, the velocity-uncertainty estimations by the third-order differentiator and the control results by the designed controller have satisfying qualities. The stochastic noises are restrained sufficiently by the differentiator and differentiation-integration observer. Furthermore, from Fig. 9, no chattering and drift phenomena happen for the differentiation-integration observer in long-time simulation. In the

tracking outputs, not only the dynamical performances are fast, but also the tracking precisions are accurate. Importantly, due to the satisfying estimate precision and the strong robustness of the observers, a very simple control law can be selected to implement the satisfying tracking qualities. However, from Figs. 8(e), 8(f), 8(g), 9(e), 9(f) and 9(g), the obvious position drifts exist in the outputs of the integral algorithm by the Extended Kalman filter. The integral algorithm can't restrain the effect of stochastic noise (especially non-white noise). Such noise leads to the accumulation of additional drift in the integrated signal.

6 Conclusions

In this paper, a generalized differentiation-integration observer has been developed, which can estimate the integrals and derivatives of a signal, synchronously. The proposed observers have built in low pass filters. It can achieve better performance without additional filters. The effectiveness of the proposed differentiation-integration observer was shown by the simulations: i) it succeeded in estimating the integrals and derivatives of the measurement signal; ii) Due to the satisfying estimate precision and the strong robustness, the differentiation-integration observers are suitable to the controller design for quadrotor aircraft. The merits of the presented differentiation-integration observer include its synchronous estimation of integrals and derivatives, simple implementation, sufficient stochastic noises rejection and almost no drift phenomenon. Although high-frequency stochastic noises and measurement errors exist, the integral and derivative estimations by the proposed observer and the tracking results by the designed controller for the quadrotor aircraft have the satisfying qualities.

ACKNOWLEDGEMENT

This work is partially supported by Research Grants Council, Hong Kong, SAR PR China under RGC16200514.

Appendix

Proof of Lemma 1: Let $\bar{k}_i = k_i$, and $\bar{k}_p = \frac{k_p}{\varepsilon^{p-c(p)}}$, where $p \neq i, i = 1, \dots, n$. Then the polynomial (5) can be rewritten as

$$s^n + \bar{k}_n s^{n-1} + \dots + \bar{k}_p s^{p-1} + \dots + \bar{k}_2 s + \bar{k}_1 \quad (61)$$

The Routh table of the polynomial (61) is presented in Fig. 10. We found that the Routh table is the nested structure.

1) when $n \in \{1, 2, \dots\}$ and $p = 1$, we know that $\bar{k}_i = k_i$, where $i = 1, \dots, n$. From the Routh table in figure 10, the parameters $k_i > 0$ (where $i = 1, \dots, n$) can be selected such that the polynomial $s^n + \sum_{i=1}^n k_i s^{i-1}$ is Hurwitz.

If there exists an integer N , such that, when $n = N$ and $p \in \{2, 3, \dots, n\}$, for the arbitrary large \bar{k}_p , the polynomial (61) cannot be Hurwitz, then, from the nested structure of the Routh table, when $n \geq N$ and $p \in \{2, 3, \dots, n\}$, for the arbitrary large \bar{k}_p , the polynomial (61) cannot be Hurwitz.

s^n	1	\bar{k}_{n-1}	\bar{k}_{n-3}	\bar{k}_{n-5}	...
s^{n-1}	\bar{k}_n	\bar{k}_{n-2}	\bar{k}_{n-4}	\bar{k}_{n-6}	...
s^{n-2}	$A_1 = \frac{\bar{k}_n \bar{k}_{n-1} - \bar{k}_{n-2}}{\bar{k}_n}$	$A_2 = \frac{\bar{k}_n \bar{k}_{n-3} - \bar{k}_{n-4}}{\bar{k}_n}$	$A_3 = \frac{\bar{k}_n \bar{k}_{n-5} - \bar{k}_{n-6}}{\bar{k}_n}$	$A_4 = \frac{\bar{k}_n \bar{k}_{n-7} - \bar{k}_{n-8}}{\bar{k}_n}$...
s^{n-3}	$B_1 = \frac{A_1 \bar{k}_{n-2} - \bar{k}_n A_2}{A_1}$	$B_2 = \frac{A_1 \bar{k}_{n-4} - \bar{k}_n A_3}{A_1}$	$B_3 = \frac{A_1 \bar{k}_{n-6} - \bar{k}_n A_4}{A_1}$	$B_4 = \frac{A_1 \bar{k}_{n-8} - \bar{k}_n A_5}{A_1}$...
s^{n-4}	$C_1 = \frac{B_1 A_2 - A_1 B_2}{B_1}$	$C_2 = \frac{B_1 A_3 - A_1 B_3}{B_1}$	$C_3 = \frac{B_1 A_4 - A_1 B_4}{B_1}$	$C_4 = \frac{B_1 A_5 - A_1 B_5}{B_1}$...
s^{n-5}	$D_1 = \frac{C_1 B_2 - B_1 C_2}{C_1}$	$D_2 = \frac{C_1 B_3 - B_1 C_3}{C_1}$	$D_3 = \frac{C_1 B_4 - B_1 C_4}{C_1}$	$D_4 = \frac{C_1 B_5 - B_1 C_5}{C_1}$...
s^{n-6}	$E_1 = \frac{D_1 C_2 - C_1 D_2}{D_1}$	$E_2 = \frac{D_1 C_3 - C_1 D_3}{D_1}$	$E_3 = \frac{D_1 C_4 - C_1 D_4}{D_1}$	$E_4 = \frac{D_1 C_5 - C_1 D_5}{D_1}$...
s^{n-7}	$F_1 = \frac{E_1 D_2 - D_1 E_2}{E_1}$	$F_2 = \frac{E_1 D_3 - D_1 E_3}{E_1}$	$F_3 = \frac{E_1 D_4 - D_1 E_4}{E_1}$	$F_4 = \frac{E_1 D_5 - D_1 E_5}{E_1}$...
...	\ddots

Figure 10 The Routh table of the polynomial (61)

2) when $n = 2$, from the Routh table in Fig. 10, the polynomial $s^2 + \bar{k}_2 s + \bar{k}_1$ is Hurwitz if $\bar{k}_2 = \frac{k_2}{\varepsilon^{2-c(2)}} > 0$ and $\bar{k}_1 = k_1 > 0$. That is to say, for the arbitrary $\varepsilon \in (0, 1)$, the polynomial $s^2 + \frac{k_2}{\varepsilon^{2-c(2)}} s + k_1$ is Hurwitz if $k_1 > 0$ and $k_2 > 0$.

3) when $n = 3$, from the Routh table in Fig. 10, the polynomial $s^3 + \bar{k}_3 s^2 + \bar{k}_2 s + \bar{k}_1$ is Hurwitz if $\bar{k}_3 > 0$, $A_1 > 0$ and $B_1 > 0$, i.e., $\bar{k}_3 > 0$, $\bar{k}_1 > 0$, and $\bar{k}_3 \bar{k}_2 > \bar{k}_1$. Therefore: i) when $p = 2$ (i.e., $\bar{k}_2 = \frac{k_2}{\varepsilon^{2-c(2)}}$), for the arbitrary $\varepsilon \in (0, 1)$, polynomial $s^3 + k_3 s^2 + \frac{k_2}{\varepsilon^{2-c(p)}} s + k_1$ is Hurwitz if $k_1 > 0$, $k_3 > 0$, $k_2 > \varepsilon^{2-c(p)} \frac{k_1}{k_3}$; ii) when when $p = 3$ (i.e., $\bar{k}_3 = \frac{k_3}{\varepsilon^{3-c(3)}}$), for the arbitrary $\varepsilon \in (0, 1)$, polynomial $s^3 + \frac{k_3}{\varepsilon^{3-c(3)}} s^2 + k_2 s + k_1$ is Hurwitz if $k_1 > 0$, $k_3 > 0$, $k_2 > \varepsilon^{3-c(3)} \frac{k_1}{k_3}$.

4) when $n = 4$, from the Routh table in Fig. 10, the polynomial $s^4 + \bar{k}_4 s^3 + \bar{k}_3 s^2 + \bar{k}_2 s + \bar{k}_1$ is Hurwitz if $\bar{k}_4 > 0$, $A_1 > 0$, $B_1 > 0$, and $C_1 > 0$, i.e., $\bar{k}_4 > 0$, $\bar{k}_4 \bar{k}_3 > \bar{k}_2$, $\frac{\bar{k}_4 \bar{k}_3 - \bar{k}_2}{\bar{k}_4} \bar{k}_2 > \bar{k}_4 \bar{k}_1$, $\bar{k}_1 > 0$. We find that, for the arbitrary $\varepsilon \in (0, 1)$, only when $p = 3$, the polynomial $s^4 + k_4 s^3 + \frac{k_3}{\varepsilon^{3-c(3)}} s^2 + k_2 s + k_1$ is Hurwitz if $k_1 > 0$, $k_4 > 0$, $k_3 > \varepsilon^{3-c(3)} \frac{k_2}{k_4}$, and $k_2 > \varepsilon^{3-c(3)} \frac{k_4^2 k_1 + k_2^2}{k_4 k_3}$.

5) when $n = 5$, from the Routh table in Fig. 10, the polynomial $s^5 + \bar{k}_5 s^4 + \bar{k}_4 s^3 + \bar{k}_3 s^2 + \bar{k}_2 s + \bar{k}_1$ is Hurwitz if $\bar{k}_5 > 0$, $A_1 > 0$, $B_1 > 0$, $C_1 > 0$, and $D_1 > 0$. We found that, for arbitrary large $\bar{k}_p = \frac{k_p}{\varepsilon^p}$ and all the $p \in \{2, 3, 4, 5\}$, no matter how to select \bar{k}_i (where $i = 1, \dots, 5$), the polynomial $s^5 + \bar{k}_5 s^4 + \bar{k}_4 s^3 + \bar{k}_3 s^2 + \bar{k}_2 s + \bar{k}_1$ cannot be Hurwitz.

6) Therefore, from the nested structure of the Routh table, there exists an integer 5, when $n \geq 5$ and $p \in \{2, 3, \dots, n\}$, for the arbitrary large $\bar{k}_p = \frac{k_p}{\varepsilon^p}$, the polynomial (5) cannot be Hurwitz. This

concludes the proof. ■

Proof of Theorem 2: In the light of Corollary 1, the observation signals is satisfied with $\lim_{\varepsilon \rightarrow 0} \widehat{p}_p = p_p$, $\lim_{\varepsilon \rightarrow 0} \widehat{\dot{p}}_p = \dot{p}_p$, $\lim_{\varepsilon \rightarrow 0} \widehat{\delta}_p = \delta_p$, where

$$p_p = \begin{bmatrix} x \\ y \\ z \end{bmatrix}, \dot{p}_p = \begin{bmatrix} \dot{x} \\ \dot{y} \\ \dot{z} \end{bmatrix}, \widehat{p}_p = \begin{bmatrix} \widehat{x} \\ \widehat{y} \\ \widehat{z} \end{bmatrix}, \widehat{\dot{p}}_p = \begin{bmatrix} \widehat{\dot{x}} \\ \widehat{\dot{y}} \\ \widehat{\dot{z}} \end{bmatrix} \quad (62)$$

Considering controller (56), the closed-loop error system for position dynamics is

$$\ddot{e}_p = -k_{p1}e_p - k_{p2}\dot{e}_p - k_{p1}(\widehat{p}_p - p_p) - k_{p2}(\widehat{\dot{p}}_p - \dot{p}_p) - m^{-1}(\widehat{\delta}_p - \delta_p) \quad (63)$$

For $t \geq t_s$ and sufficiently small ε , selecting the Lyapunov function be $V_p = k_{p1}e_p^T e_p + \frac{1}{2}\dot{e}_p^T \dot{e}_p$, we can obtain that $e_p \rightarrow 0$ and $\dot{e}_p \rightarrow 0$ as $t \rightarrow \infty$. This concludes the proof. ■

Proof of Theorem 3: In the light of Corollary 2, the observation signals is satisfied with $\lim_{\varepsilon \rightarrow 0} \widehat{p}_a = p_a$, $\lim_{\varepsilon \rightarrow 0} \widehat{\dot{p}}_a = \dot{p}_a$, $\lim_{\varepsilon \rightarrow 0} \widehat{\delta}_a = \delta_a$, where

$$a_a = \begin{bmatrix} \psi \\ \theta \\ \phi \end{bmatrix}, \dot{a}_a = \begin{bmatrix} \dot{\psi} \\ \dot{\theta} \\ \dot{\phi} \end{bmatrix}, \widehat{a}_a = \begin{bmatrix} \widehat{\psi} \\ \widehat{\theta} \\ \widehat{\phi} \end{bmatrix}, \widehat{\dot{a}}_a = \begin{bmatrix} \widehat{\dot{\psi}} \\ \widehat{\dot{\theta}} \\ \widehat{\dot{\phi}} \end{bmatrix} \quad (64)$$

Considering controller (59), the closed-loop error system for attitude dynamics is

$$\ddot{e}_a = -k_{a1}e_a - k_{a2}\dot{e}_a - k_{a1}(\widehat{a}_a - a_a) - k_{a2}(\widehat{\dot{a}}_a - \dot{a}_a) - J^{-1}(\widehat{\delta}_a - \delta_a) \quad (65)$$

For $t \geq t_s$ and sufficiently small ε , selecting the Lyapunov function be $V_a = k_{a1}e_a^T e_a + \frac{1}{2}\dot{e}_a^T \dot{e}_a$, we can obtain that $e_a \rightarrow 0$ and $\dot{e}_a \rightarrow 0$ as $t \rightarrow \infty$. This concludes the proof. ■

References

- [1] S.-C. Pei, and J.-J. Shyu (1989). Design of FIR Hilbert Transformers and differentiators by eigenfilter. IEEE Trans. Acoust. Speech Signal Process., ASSP(37), 505-511.
- [2] A. N. Atassi and H. K. Khalil (2000). Separation results for the stabilization of nonlinear systems using different high-gain observer designs. Systems and Control Letters, 39, 183-191.
- [3] S. Ibrir (2004). Linear time-derivative trackers. Automatica Vol. 40, 397-405.
- [4] A. Levant (1998). Robust exact differentiation via sliding mode technique. Automatica, vol. 34, no. 3, 379-384.
- [5] A. Levant (2003). High-order sliding modes, differentiation and output-feedback control. International Journal of Control, vol. 76, Nos. 9/10, 924-941.

- [6] X. Wang, Z. Chen, and G. Yang (2007). Finite-time-convergent differentiator based on singular perturbation technique. *IEEE Transactions on Automatic Control*, Vol. 52, No. 9, 1731-1737.
- [7] X. Wang and B. Shirinzadeh (2012). Rapid-convergent nonlinear differentiator. *Mechanical Systems and Signal Processing*, Vol. 28, 414-431.
- [8] X. and B. Shirinzadeh (2014). High-order nonlinear differentiator and application to aircraft control, *Mechanical Systems and Signal Processing*, vol. 46, no. 2, pp. 227-252.
- [9] X. Wang, H. Lin (2012). Design and frequency analysis of continuous finite-time-convergent differentiator, *Aerospace Science and Technology*, vol. 18, no. 1, 69-78.
- [10] D. V. Efimov and L. Fridman (2011). A hybrid robust non-homogeneous finite-time differentiator. *IEEE Transactions on Automatic Control*, Vol. 56, No. 5, 1213-1219.
- [11] B. H. Hahn, D. T. Valentine (2010). *Essential MATLAB for Engineers and Scientists*, 4nd ed Elsevier Ltd.
- [12] C. C. Tseng (2006). Digital integrator design using Simpson rule and fractional delay filter. *IEE Proceedings - Vision, Image and Signal Processing*, Vol. 153 No. 1, 79 - 86.
- [13] C. C. Tseng, S. L. Lee (2008). Digital IIR integrator design using recursive Romberg integration rule and fractional sample delay. *Signal Processing*, Vol. 88, No. 9, 2222-2233.
- [14] N. Q. Ngo (2006). A new approach for the design of wideband digital integrator and differentiator. *IEEE Transactions on Circuits and Systems II: Express Briefs*, Vol. 53, No. 9 On page(s): 936-940.
- [15] T. Hodges, P.A. Nelson, S.J. Elliott (1990). The design of a precision digital integrator for use in an active vibration control system. *Mechanical Systems and Signal Processing*, Vol. 4, No. 4, 345-353.
- [16] M. A. Al-Alaoui (1989). A novel approach to designing a noninverting integrator with built-in low frequency stability, high frequency compensation, and high Q. *IEEE Transactions on Instrumentation and Measurement*, Vol. 38, No. 6, 1116 - 1121.
- [17] M. A. Al-Alaoui (1993). Novel digital integrator and differentiator. *Electronics Letters*, Vol. 29 No. 4, 376 - 378.
- [18] M. A. Al-Alaoui (1995). A Class of Second Order Integrators and Lowpass Differentiators. *IEEE Transactions on Circuits and Systems—I: Fundamental Theory and Applications*, Vol. 42, No. 4, 220-223.
- [19] M. A. Al-Alaoui (2001). Low-frequency differentiators and integrators for biomedical and seismic signals, *IEEE Transactions on Circuits and Systems—I: Fundamental Theory and Applications*, Vol. 48, No. 8, 1006-1011.
- [20] M. A. Al-Alaoui (2011). Class of digital integrators and differentiators. *IET Signal Process.* Vol. 5, No. 2, 251–260.

- [21] A. Charef, H. H. Sun, Y. Y. Tsao, and B. Onaral (1992). Fractal system as represented by singularity function, *IEEE Transactions on Automatic Control*, Vol. 37, No. 9, 1465-1470.
- [22] A. Chiaref (2006). Analogue realisation of fractional-order integrator, differentiator and fractional $PI^\lambda D^\mu$ controller, *IEE Proc. - Control Theory Appl.*, Vol. 153, No. 6, 714-720.
- [23] L. Idkhajine, E. Monmasson, and A. Maalouf (2012). Fully FPGA-based sensorless control for synchronous AC drive using an extended Kalman filter, *IEEE Transactions on Industrial Electronics*, vol. 59, no. 10, pp. 3908-3918.
- [24] X. Wang, B. Shirinzadeh, and M.H. Ang, Jr (2015). Nonlinear double-integral observer and application to quadrotor aircraft, *IEEE Transactions on Industrial Electronics*, vol. 62, no. 2, 1189-1200.
- [25] X. Wang and B. Shirinzadeh (2014). Nonlinear multiple integrator and application to aircraft navigation, *IEEE Transactions on Aerospace and Electronic Systems*, vol. 50, no. 1, pp. 607-622.
- [26] X. Wang and B. Shirinzadeh (2014). Nonlinear continuous integral-derivative observer, *Nonlinear Dynamics*, vol. 77, no. 3, pp. 793-806.
- [27] Ju-Il Lee and In-Joong Ha (2002), A novel approach to control of nonminimum-phase nonlinear systems, *IEEE Trans. Automat. Contr.*, vol., 47, pp. 1480-1486.
- [28] H. Kahlil (2002), *Nonlinear systems*, 3rd ed. Englewood Cliffs, New Jerse: Prentice-Hall.
- [29] X. Wang, B. Shirinzadeh (2015). Nonlinear augmented observer design and application to quadrotor aircraft, *Nonlinear Dynamics*, vol. 80, no. 3, 1463-1481.
- [30] F. Kendoul, D. Lara, I. Fantoni-Coichot, and R. Lozano (2007). Real-time nonlinear embedded control for an autonomous quadrotor helicopter, *Journal of Guidance, Control, and Dynamics*, vol. 30, no. 4, pp. 1049-1061, Jul.-Aug.
- [31] L.R. Carrillo, A. Dzul, R. Lozano, (2012). Hovering quad-rotor control: a Comparison of nonlinear controllers using visual feedback. *IEEE Transactions on Aerospace and Electronic Systems*, 48(4), 3159–3170.
- [32] D. Lee, H. Lim, H.J. Kim, Y. Kim, K.J. Seong (2012). Adaptive image-based visual servoing for an underactuated quadrotor system. *Journal of Guidance, Control and Dynamics*, 35(4), 1335–1353.
- [33] A. Chamseddine, Y. Zhang, C. A. Rabbath, C. Join, D. Theilliol ((2012)). Flatness-Based trajectory planning/replanning for a quadrotor unmanned aerial vehicle. *IEEE Transactions on Aerospace and Electronic Systems*, 48(4), 2832–2848.
- [34] S. Grzonka, G. Grisetti, and W. Burgard (2009). Towards a navigation system for autonomous indoor flying, in *IEEE Int. Conf. on Robotics and Automation*, Kobc, Japan, May 12-17, pp. 2878-2883.
- [35] X. Wang, Z. Chen, and Z. Yuan (2003). Design and analysis for new discrete tracking-differentiators, *Applied Mathematics-A Journal of Chinese Universities*, vol. 18, no. 2, 214-222.